A UNIFIED TECHNIQUE FOR DYNAMIC MODELING AND STABILITY ANALYSIS OF MICROGRID SYSTEMS

BY

BRIAN BENJAMIN JOHNSON

THESIS

Submitted in partial fulfillment of the requirements
for the degree of Master of Science in Electrical and Computer Engineering
in the Graduate College of the
University of Illinois at Urbana-Champaign, 2009

Urbana, Illinois

Adviser:

Associate Professor Patrick L. Chapman

ABSTRACT

This work presents a unified method for dynamic modeling and stability analysis of microgrid power systems. Using the automated state-model generation algorithm, a state-space model of the microgrid power system is derived. The model may be used to conduct time-domain simulations and analyze system response to large transients. Additionally, eigenvalues of the system may be analyzed with respect to inverter control gains to assess small-signal stability. The proposed methodology is verified for large-signal transient study and small-signal stability analysis using dual and single-inverter microgrid systems, respectively. The presented method is general and may be applied to any three-phase circuit topology and inverter control without the need to derive circuit state equations.

To my family, friends, and loved ones for all their support

ACKNOWLEDGMENTS

I would like to thank my adviser, Professor Patrick Chapman, for giving me the opportunity to pursue graduate studies here at the University of Illinois at Urbana-Champaign. I would also like to thank Professor Peter Sauer for helping me complete this research.

This work was supported by The Graduate College Fellowship and SURGE Fellowship. Additionally, this research was sponsored by Odyssian Technology and USACE CERL on an STTR Phase I subcontract funded by the US Army on prime contract W9132T-08-C-0037.

The views, opinions, and findings contained in this document are those of the author and should not be construed as an official U.S. Department of Defense position, policy, or decision.

TABLE OF CONTENTS

CHAPTER 1

INTRODUCTION

A microgrid is a system composed of distributed energy sources located near loads of interest that is capable of independent control. Generally, microgrids are able to island from the main grid to provide uninterruptible power to the local loads [1]. A wide variety of energy sources including gas turbines, photovoltaics, wind turbines, and batteries may be integrated into the system. The ac energy sources in the microgrid are rectified and connected to dc buses while dc power sources are interfaced to the dc buses through dc-dc converters. A three-phase voltage-source inverter interfaces each dc bus with the ac microgrid bus [2], as shown in Figure 1.1. Microgrids are typically implemented in mission-critical systems, and consequently their stability assessment and large-signal transient analysis are of particular interest, e.g., to study system stability during large transient events such as islanding. Additionally, it is useful to perform small-signal stability analysis with respect to the inverter control parameters to determine the relationship between control settings and stability during small disturbances. Therefore, there has been growing interest in computer-aided dynamic characterization of microgrid power systems for large signal transient study, stability analysis, and controller design [3], [4], [5].

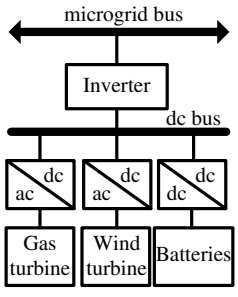

Figure 1.1: Power electronic interface to microgrid

1.1 Previous Work in Microgrid Modeling and Analysis

Power circuit simulators generally fall into two categories: nodal-variable and state-variable based languages [6]. Nodal models are described using circuit elements and branch parameters. Difference equations are established to relate the circuit variables at the current time step to those at the previous one. The equations describing the system are then solved numerically using techniques such as Runge-Kutta, Euler, or trapezoid [7], [8]. Using the nodal method, the analyst is relieved of formulating the state equations of a possibly complex circuit. However, since composite system equations are never established, few system-level analysis techniques are available.

Nodal based simulators such as ElectroMagnetic Transients Program (EMTP), Alternative Transients Program (ATP), and Power Systems Computer Aided Design (PSCAD) have been used extensively to model microgrids and distributed energy systems. Nodal-based simulation packages similar to EMTP are based on an admittance matrix description of the system and generally use trapezoidal integration with a small fixed-step size [9], [10]. Using these software packages, the stability of microgrid systems can be assessed by conducting time-domain simulations of the disturbances and transients the analyst wishes to evaluate. This analysis gives insight into the system response and has been widely used to analyze large transients such as faults and system islanding [11]. Unfortunately, this method does not allow for eigenvalue analysis [10] and often requires separate models for system components [12]. In order to gain insight into the relationship between the system eigenvalues and control parameters, a state-variable based simulation must be used.

To establish a state-variable model, differential equations describing the system must be established by the analyst [8]. State equations may be programmed or the equations may be represented graphically using a block diagram. These equations may then be solved using a variety of available integration schemes. The equations describing the system may be formulated into a state-space model and analyzed using a variety of techniques. For stability analysis, the model may be linearized and the system eigenvalues may be evaluated with respect to the control and circuit parameters. A disadvantage to this approach is that the differential

equations of the circuit must be formulated, and this becomes a tedious task for complex circuits [7].

State-space modeling of microgrids has been used to evaluate the small-signal system stability with respect to control and circuit parameters [13]. As shown in [4], a linearized model of the system may be derived so that the system-level eigenvalues may be analyzed. However, this method requires the separate formulation of state-space models for the inverters, network, and loads. Additionally, since these models are linearized, they are only valid for small signals and cannot be used to model system response under all conditions. State-variable models of microgrids have also been established graphically using Simulink [14], [3]. Although some of these models may be valid for large disturbances [15], they also require significant effort to formulate the system component models and system equations.

1.2 Proposed Approach

The automated state model generation (ASMG) algorithm [7] combines the benefits of both nodal-variable and state-variable based approaches. Using ASMG, a system is described by pertinent branch parameters and circuit topology. Composite system state equations are established systematically and there is no need to formulate the differential equations explicitly. The proposed methodology is systematic and therefore automatable. This algorithm has been previously demonstrated to be effective for simulating switched networks such as motor drives and switching converters. It has also been accelerated and improved to enhance ease of implementation and computational performance [16], [17].

This work is focused on the development of a unified technique which allows for both time-domain simulations of large transients and small-signal stability analysis. Using ASMG, a state-space model of a microgrid power system is formulated and used to conduct a detailed simulation of system transient response. This capability may be used to assess the stability of the system in regard to faults, load changes, grid disturbances, or any large disturbance of interest. The state-space model may then be linearized so that the eigenvalues may be analyzed at the system level [18] with respect to the inverter control parameters. This analysis will provide insight into

the relationship between inverter control settings and system stability. The proposed method is verified for both large-transient and small-signal stability case studies for both dual and single inverter systems, respectively.

CHAPTER 2

MICROGRID CHARACTERISTICS AND INVERTER MODELING

There have been several coordinated efforts to design and implement microgrid installations. In the United States, organizations such as the Consortium for Electric Reliability Technology Solutions (CERTS), Northern Power Systems, and General Electric have constructed operational microgrids. Additionally, several microgrids have also been constructed in the European Union and in Asia [19]. As each of these installations utilizes different energy sources and control methods, it would be outside the scope of this work to examine each system. This work will focus on the techniques used in the CERTS microgrid installation.

Regardless of the type of microgrid investigated, each cluster of distributed generation (DG) energy sources and its power electronic interface, collectively referred to as a microsource, must use a control system that maintains stable operation during grid-connected and islanded modes. Generally, the control methods fall into two categories: peer-to-peer and master-slave controls. One implementation of master-slave control requires the use of a single microsource acting as the master. The master microsource then regulates the voltage and frequency of the microgrid. Alternatively, a centralized controller may be used to send voltage, power, and other settings to all microsources [20]. Because there is a master controller, this type of system has a single point of failure.

Peer-to-peer control is a method where each microsource has a dedicated controller and communication is not required between the DG sources. Incorporation of additional energy sources does not require system redesign and the microgrid becomes plug-and-play. As long as the load demand can be met, operation is maintained despite the failure of any microsource [1], [21]. Discussion will be limited to peer-to-peer control. The CERTS microgrid, as shown in Figure 2.1, uses this type of control system. The system uses a static three-phase switch to separate the microgrid from the

utility in the event of grid disturbances [22].

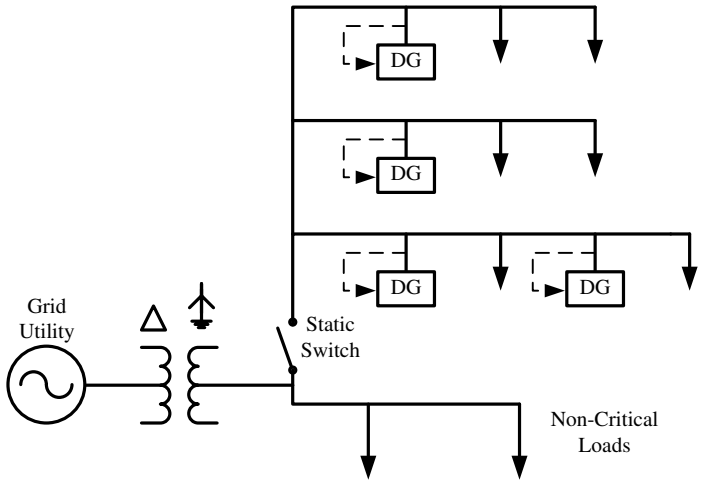

Figure 2.1: CERTS microgrid installation

2.1 Operational Modes

2.1.1 Grid-connected

When the microgrid is connected to the grid utility, the system voltage will be predominantly influenced by the stiff voltage of the utility. Thus, the microsources have little influence over the microgrid voltage [23] and they instead act as power regulators. During grid-connected mode, the DG inverters can regulate either the power supplied by each microsource or the power imported from the utility [5], [24]. When the power supplied by each microsource is regulated, each inverter injects a fixed amount of power into the microgrid system. This is referred to as *unit power control* [22] and it is achieved when the measurements shown in Figure 2.1 are utilized. If the DG sources produce more power than is required by the loads, then the excess power will be exported to the utility. Conversely, if the power supplied by the DG sources is insufficient to meet load demand, power will be imported to the microgrid. Thus, the amount of power supplied by or injected into the grid is dependent on the load demand in the microgrid.

Alternatively, feeder-flow control is used to control the total power

imported by the utility [22]. Using this method, the microgrid behaves as a constant load to the utility grid. The type of control is achieved when the DG sources utilize the feeder voltage and current measurements. In order to regulate the feeder power flow in the midst of load fluctuations, the power injected into the feeder by the inverters will be dynamic. It is also possible to have a hybrid system where some microsources use feeder-flow control and others use unit-power control.

2.1.2 Islanded

After the system is islanded, the microgrid no longer has the voltage support of the utility grid. In this scenario, the DG controllers regulate their output voltage to provide a seamless voltage magnitude during the transition to islanding. This mode of operation is often referred to as *voltage control mode* [24]. The power supplied to the local loads will be uninterrupted because the microsources are capable of rapid increases in power delivery. A power vs. frequency droop is used to maintain system stability under a unified system frequency [2], [25].

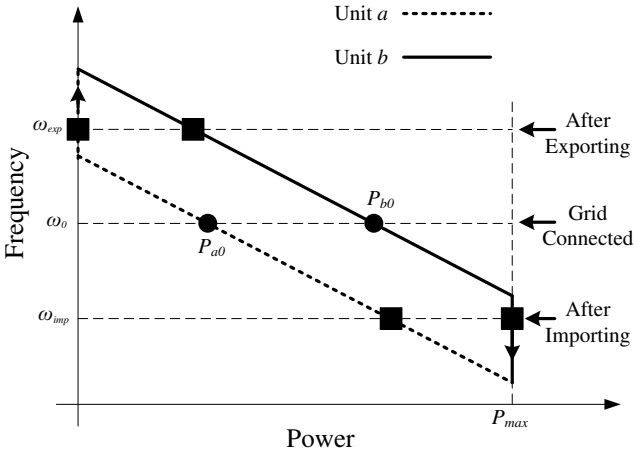

Figure 2.2: Power vs. frequency droop

Figure 2.2 shows the relationship between power and frequency for each DG unit. Analogous to the $P - \omega$ relationship exhibited by synchronous generators, the frequency will decrease as power output increases and vice versa. Since the system must maintain a unified frequency, all microsources will have the same frequency. The graph in Figure 2.2 shows the $P - \omega$

curves of two microsources in a system using unit-power control. Initially, the system is operating at the synchronous frequency, ω_0, while grid-connected and Units a and b are producing powers P_{a0} and P_{b0}. If the microgrid is importing power from the grid before islanding, then the power output of the microsources must increase to accommodate the load once islanded. In this case, the system frequency will decrease to a steady-state value of ω_{imp} as the microsource power increases. Conversely, if the microgrid was initially exporting power before islanding, the microsources must decrease their power output. In this case, the system frequency will increase to ω_{exp}. There are maximum power , $P_{\max}$, and minimum power output limits that also must be enforced. For example, if the power output of Unit b reaches $P_{\max}$, then it will be held at $P_{\max}$ as the frequency continues to vary (Figure 2.2). Similar behavior occurs for Unit a as the power output decreases. The $P - \omega$ curves for feeder-flow control are nearly identical to Figure 2.2, with the exception that power flow can be negative as well as positive [22].

2.2 Energy Sources and Inverter Model

Each inverter interfaces the ac microgrid to a dc bus fed by several energy sources. As one of the primary aims of the microgrid is to achieve a highly reliable supply of power, a wide variety of independent energy sources is connected to each dc bus [26]. Because the dynamic response of energy sources such as fuel cells, gas turbines, diesel generators, and wind turbines varies widely, energy storage capable of rapid changes in power output must be used. In a typical installation, a diesel generator may supply the base load while batteries supply and store power during transients. Sophisticated methods for managing battery charging and the interaction of energy sources have been established [2]. For purposes of modeling the output of the inverter, it may be assumed that the dc bus voltage magnitude is fixed and that the power demand may be satisfied.

The ideal dc bus, filtered inverter output $\mathbf{e}_{\text{inv}(abc)}(t)$, and closed-loop control can be be modeled as shown in Figure 2.3. Each inverter in the CERTS microgrid is connected to the ac microgrid bus through an added inductance L_{inv} and three-phase delta to wye transformer. As shown, the

controller is configured for unit-power control and will regulate the measured quantities at the point of connection with the microgrid bus. Measured voltages and currents, $\mathbf{v}_{abc}(t)$, and, $\mathbf{i}_{abc}(t)$, are transformed to the $qd0$ reference frame and used to calculate the real power, $\tilde{P}$, reactive power, $\tilde{Q}$, and RMS voltage, $\tilde{V}$, using (2.1)-(2.3). The inverter model is non-linear because of the $\tilde{P}$, $\tilde{Q}$, and $\tilde{V}$ calculations.

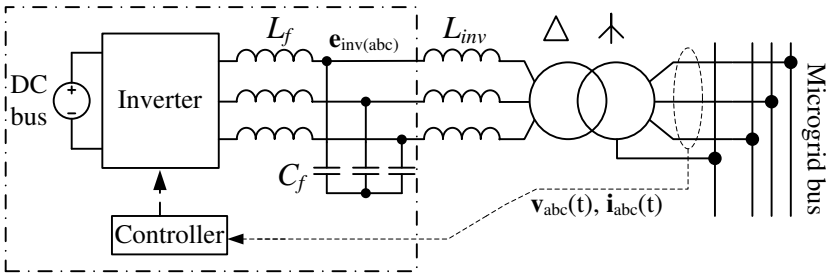

Figure 2.3: Inverter model and closed-loop control

$$\tilde{P} = \frac{3}{2}(V_d I_d + V_q I_q + 2V_0 I_0) \tag{2.1}$$

$$\tilde{Q} = \frac{3}{2}(V_d I_q - V_q I_d) \tag{2.2}$$

$$\tilde{V} = \sqrt{V_d^2 + V_q^2} \tag{2.3}$$

2.2.1 State equations

A block diagram of the inverter control is shown in Figure 2.4. The user-defined commands are the rms voltage V^* and power P^*. Minimum and maximum power capabilities, $P_{\min}$ and $P_{\max}$, are also defined so that the physical limits of the microsource are enforced. Neglecting switching ripple, the outputs $|E_{\text{inv}}|$ and θ_v are used to control the inverter gate signals to create a filtered inverter output voltage that satisfies (2.4). The presented equations model behavior of the dashed box in Figure 2.3.

$$\mathbf{e}_{\text{inv}(abc)}(t) = |E_{\text{inv}}| \begin{bmatrix} \cos(\theta_v(t)) \\ \cos(\theta_v(t) - \frac{2\pi}{3}) \\ \cos(\theta_v(t) + \frac{2\pi}{3}) \end{bmatrix} \tag{2.4}$$

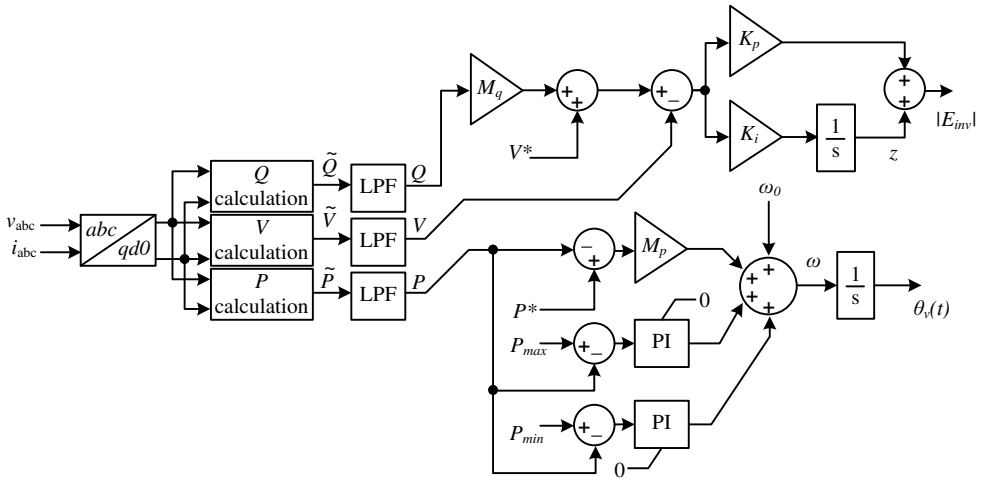

Figure 2.4: Inverter control block diagram

The power vs. frequency droop control is enforced by the lower control loop in the block diagram in Figure 2.4. The upper control loop enforces voltage vs. reactive power droop control to prevent reactive power oscillations between multiple microsources and excessive currents [22]. Each inverter control system model has a total of seven state variables. However, only the five state variables P, Q, V, θ_v, and z will be non-zero when the power output is within the limits $P_{\max}$ and $P_{\min}$. P, Q, and V are filtered quantities that are free of extraneous high-frequency content and z is defined as the output of the V-vs.-Q droop integrator. The P, Q, and V low-pass filter time constants are denoted as τ_P, τ_Q, and τ_V, respectively, and the differential equations describing P, Q, V, θ_v, and z are summarized in (2.5)-(2.9). A voltage base, V_{base}, and system power base, S_{base}, must be established.

$$\dot{P} = \frac{\tilde{P} - P}{\tau_P} \tag{2.5}$$

$$\dot{Q} = \frac{\tilde{Q} - Q}{\tau_Q} \tag{2.6}$$

$$\dot{V} = \frac{\tilde{V} - V}{\tau_V} \tag{2.7}$$

$$\dot{\theta_v} = M_p(P^* - P) \tag{2.8}$$

$$\dot{z} = K_i \left(\frac{QM_q}{S_{\text{base}}} + E^* - \frac{V}{V_{\text{base}}} \right) \tag{2.9}$$

Using the block diagram in Figure 2.4, the inverter voltage magnitude, $|E_{\text{inv}}|$, may be written as

$$|E_{\text{inv}}| = z + K_p \left(\frac{QM_q}{S_{\text{base}}} + E^* - \frac{V}{V_{\text{base}}} \right) \tag{2.10}$$

and $\mathbf{e}_{\text{inv}(abc)}$ may now be expressed in terms of the defined state-variables.

$$\mathbf{e}_{\text{inv}(abc)}(t) = \left(z + K_p \left(\frac{QM_q}{S_{\text{base}}} + E^* - \frac{V}{V_{\text{base}}} \right) \right) \begin{bmatrix} \cos(\theta_v(t)) \\ \cos(\theta_v(t) - \frac{2\pi}{3}) \\ \cos(\theta_v(t) + \frac{2\pi}{3}) \end{bmatrix} \tag{2.11}$$

The presented inverter model may be used to simulate the dynamics of each microsource in a microgrid system. However, in order to develop a complete microgrid model, the network, transformers, and loads must also be modeled. In Chapter 3, the modeling algorithm used to develop a unified system model will be described.

CHAPTER 3

LARGE-SIGNAL MODEL DEVELOPMENT

The microgrid is represented as a collection of n nodes and b branches using a directed graph. Using variations of an elementary branch model, commonly used linear circuit elements and switching devices in power systems can be constructed. Thus, it is possible to model transmission conductors, transformers, the utility grid, and three-phase switches. Using the additional capability that the voltage and current sources can be non-linear functions of time and other variables, the voltage source inverter average model presented in the previous chapter may be represented as a state variable dependent voltage source.

3.1 Transformers

Each microsource inverter and the infinite bus are interfaced to the microgrid with a delta to grounded-wye transformer. Before describing the three-phase transformer model, it is instructive to first consider the single-phase transformer shown in Figure 3.1. Each coil has an intrinsic resistance r, self-inductance L, and both coils are coupled with a mutual inductance M. The differential equations describing the mutually coupled circuits are shown in (3.1) [27].

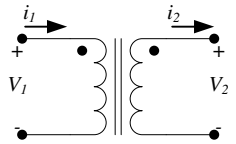

Figure 3.1: Single phase ideal transformer

$$
\begin{aligned}
v_1 &= i_1 r_1 + L_{11}\frac{di_1}{dt} - M\frac{di_2}{dt} \\
v_2 &= i_2 r_2 + L_{22}\frac{di_2}{dt} - M\frac{di_1}{dt}
\end{aligned}
\tag{3.1}
$$

The self-inductance of each coil, L_{11} and L_{22}, is the sum of leakage and magnetizing terms, L_l, and, L_m, respectively. Leakage inductances are related to the turns ratio using (3.2) and mutual inductance can be expressed in terms of the magnetizing inductances using (3.3) [28].

$$
\frac{N_1}{N_2} = \frac{L_{l1}}{L_{l2}} \tag{3.2}
$$

$$
M = \sqrt{L_{m1} L_{m2}} \tag{3.3}
$$

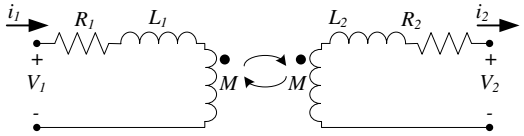

Figure 3.2: Single-phase transformer model

The non-ideal single-phase transformer can be modeled as the coupled circuits shown in Figure 3.2. Using the established results, the three-phase phase delta to grounded-wye transformer can be constructed using three single-phase transformer models, as shown in Figure 3.3. Essentially, the model has three pairs of coupled circuits where each pair has a $\frac{V_{\Delta(\mathrm{LL})}}{V_{\mathrm{Y(LN)}}} = \frac{480}{120} = \frac{N_\Delta}{N_\mathrm{Y}}$ turns ratio. The self-inductances can be expressed using (3.4).

$$
\begin{aligned}
L_\Delta &= L_{m\Delta} + L_{l\Delta} \\
L_\mathrm{Y} &= L_{m\mathrm{Y}} + L_{l\mathrm{Y}}
\end{aligned}
\tag{3.4}
$$

Provided transformer data generally includes S_{rated}; the rated voltages, $V_{\Delta(\mathrm{LL})}$ and $V_{\mathrm{Y(LN)}}$; the resistances, R_Δ and R_Y; and the leakage inductance of both sides in terms of the base impedance, $L_l = kZ_{\mathrm{rated}}$, where k

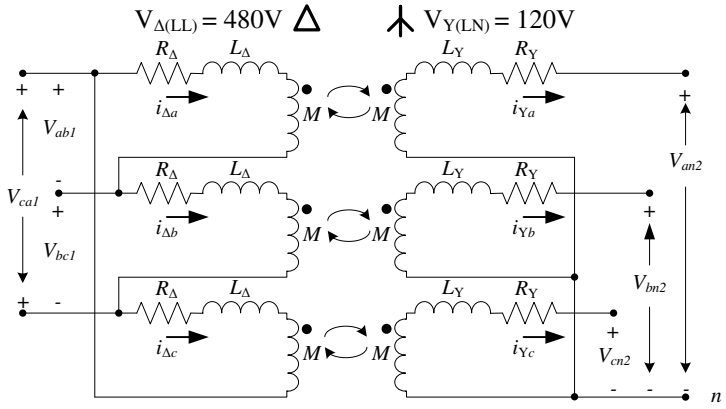

Figure 3.3: Three-phase transformer model

typically ranges from 0.01 to 0.05. The calculation for both leakage inductances, $L_{l\Delta}$ and $L_{l\mathrm{Y}}$, is shown in (3.5).

$$\begin{aligned} L_{l\Delta} &= kZ_{rated\Delta} = \frac{kV^2_{\Delta(LL)}}{S_{\text{rated}}} \\ L_{l\mathrm{Y}} &= kZ_{\text{ratedY}} = \frac{kV^2_{\mathrm{Y(LN)}}}{S_{\text{rated}}} \end{aligned} \tag{3.5}$$

Since the magnetizing inductance is not typically provided, it may be estimated that $L_M = 1000L_l$ for both sides. The mutual inductance, M, can now be calculated using (3.6).

$$M = \sqrt{L_{m\Delta}L_{mY}} = 1000\sqrt{L_{l\Delta}L_{lY}} \tag{3.6}$$

The delta to wye transformer model is now complete. The high-voltage inverters with $V_{\text{LL}} = 480$ V are interfaced to the delta side of each transformer, and the low-voltage 4-wire microgrid system with $V_{\text{LN}} = 120$ V is interfaced to the wye side. A delta to wye transformer is also used at the point of connection with the utility grid. The microgrid system is grounded via the fourth wire at the microgrid-utility transformer.

3.2 Grid-Utility and Components

As depicted in Figure 3.4, the grid utility is modeled as an equivalent impedance and a wye-connected balanced three-phase voltage-source $\mathbf{e}_{\infty(abc)}(t)$ with fixed magnitude, $V_{\text{pk(LN)}}$, and frequency, $\omega_0 = 2\pi 60$ rad/s. The infinite-bus voltages are calculated using (3.7).

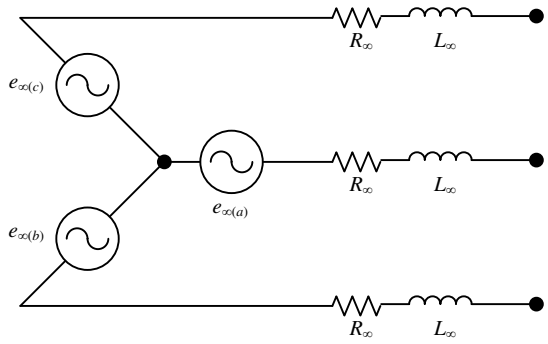

Figure 3.4: Infinite-bus model

$$\mathbf{e}_{\infty(abc)}(t) = |V_{\text{pk(LN)}}| \begin{bmatrix} \cos(\omega_0 t) \\ \cos(\omega_0 t - \frac{2\pi}{3}) \\ \cos(\omega_0 t + \frac{2\pi}{3}) \end{bmatrix} \tag{3.7}$$

The CERTS microgrid loads are purely resistive and transmission lines are modeled as branches containing a series resistance and inductance. Additional branches can be used to model lumped shunt capacitances at each end of the transmission line.

3.3 Automated State Model Generation Algorithm

Each branch in the microgrid circuit can be depicted as a variation of the elementary branch model shown in Figure 3.5. Defining $P_i = \frac{1}{C_i}$ as the reciprocal of the branch capacitance, i_i as the branch current, r_i as branch resistance, L_i as branch inductance, e_i as a voltage source, and j_i as a current source, the voltage v_i of each branch may be expressed using (3.8). The voltage and current sources, e_i and j_i, may be functions of time or other variables. Throughout the remaining chapters, p and $1/p$ will denote differentiation and integration with respect to time, respectively.

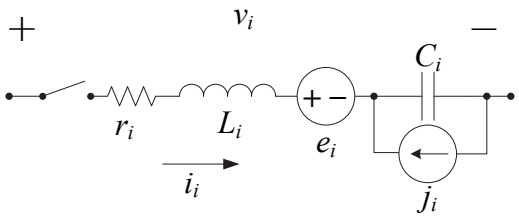

Figure 3.5: Elementary branch model

$$v_i = i_i r_i + p(L_i i_i) + P_i \frac{1}{p}(i_i + j_i) + e_i \tag{3.8}$$

Using the branch model, the transformers, loads, transmission lines, and voltage sources can be modeled as an interconnected branch network whose structure is described by the $b \times n$ node-incidence matrix $\mathbf{A}_a$. Each column of $\mathbf{A}_a$ corresponds to a branch and will have exactly two non-zero entries, with one equal to $+1$, and the other to -1. A $+1$ at the (i, j) entry of $\mathbf{A}_a$ indicates the connection of the positive terminal of the j^{th} branch to the i^{th} node. The -1 entry corresponds to the negative terminal connection. After row operations and possible re-numbering of the branches, $\mathbf{A}_a$ may be expressed as (3.9) [8].

$$\tilde{\mathbf{A}}_a = \begin{bmatrix} \mathbf{I}_{(n-1)\times(n-1)} & \hat{\mathbf{A}}_{(n-1)\times(b-n+1)} \\ \mathbf{0}_{1\times(n-1)} & \mathbf{0}_{1\times(b-n+1)} \end{bmatrix} \tag{3.9}$$

The matrix $\tilde{\mathbf{A}}$ is defined by omitting the bottom row of zeros in $\tilde{\mathbf{A}}_a$. Using $\tilde{\mathbf{A}}$, Kirchoff's current law (KCL) may be expressed as (3.10).

$$\mathbf{0} = \tilde{\mathbf{A}}\ \mathbf{i}_{br} = \begin{bmatrix} \mathbf{I} & \hat{\mathbf{A}} \end{bmatrix} \begin{bmatrix} \mathbf{i}_y \\ \mathbf{i}_x \end{bmatrix} \tag{3.10}$$

The vector composed of the branch currents, $\mathbf{i}_{br}$, may be partitioned into state-variable currents and dependent branch currents, $\mathbf{i}_x$ and $\mathbf{i}_y$, respectively. The dependent currents, $\mathbf{i}_y$, may be algebraically expressed in terms of the state-variable currents, $\mathbf{i}_x$. By rearranging (3.10), $\mathbf{i}_y$ may be calculated using (3.11).

$$\mathbf{i}_y = -\hat{\mathbf{A}}\mathbf{i}_x \tag{3.11}$$

Now, $\mathbf{i}_{br}$ may be rewritten as

$$\mathbf{i}_{br} = \begin{bmatrix} \mathbf{i}_y \\ \mathbf{i}_x \end{bmatrix} = \begin{bmatrix} -\hat{\mathbf{A}} \\ \mathbf{I} \end{bmatrix} \mathbf{i}_x = \mathbf{B}_b^T \mathbf{i}_x \tag{3.12}$$

where the branch currents, $\mathbf{i}_{br}$, can be related to the state-variable currents, $\mathbf{i}_x$, using $\mathbf{B}_b$ [7]. It can also be proven that Kirchoff's voltage law (KVL) may be expressed as $\mathbf{B}_b \mathbf{v}_{br} = \mathbf{0}$, where $\mathbf{v}_{br}$ is a vector composed of the branch voltages [8], [7].

Using the established results, it is possible to derive a state-space model of the microgrid given the node incidence matrix $\mathbf{A}_a$ and branch parameters. The branch voltage equation in (3.8) can be written in the matrix form

$$\mathbf{v}_{br} = \mathbf{r}_{br}\mathbf{i}_{br} + p(\mathbf{L}_{br}\mathbf{i}_{br}) + \mathbf{P}_{br}\frac{1}{p}(\mathbf{i}_{br} + \mathbf{j}_{br}) + \mathbf{e}_{br} \tag{3.13}$$

where the parameters of each branch r_i, L_i, and P_i constitute the $b \times b$ matrices $\mathbf{r}_{br}$, $\mathbf{L}_{br}$, and $\mathbf{P}_{br}$, respectively. The diagonal matrix $\mathbf{r}_{br}$ contains the branch resistances. Mutual inductance between transformer branches is represented in the symmetric off-diagonal entries of $\mathbf{L}_{br}$. It should be noted that although the ASMG algorithm is well suited to model mutually coupled circuits, it cannot be used to model ideal transformers because they do not have resistance and inductance. After manipulating the expression in (3.13), it is possible to describe the microgrid circuit using the state-space model shown in (3.14) - (3.15) [7]. The presented equations take the form $p\mathbf{x} = \mathbf{A}\mathbf{x} + \mathbf{B}\mathbf{u}$ and $\mathbf{y} = \mathbf{C}\mathbf{x} + \mathbf{D}\mathbf{u}$, where $\mathbf{x} = \begin{bmatrix} \mathbf{q}_c & \mathbf{i}_x \end{bmatrix}^T$ is a vector of the state-variables, $\mathbf{u} = \begin{bmatrix} \mathbf{j}_{br} & \mathbf{e}_{br} \end{bmatrix}^T$ is a vector of the inputs, and $\mathbf{y} = \begin{bmatrix} \mathbf{i}_{br} & \mathbf{v}_{br} \end{bmatrix}^T$ is the output. The matrices $\mathbf{A}$, $\mathbf{B}$, $\mathbf{C}$, and $\mathbf{D}$ can be defined by inspection.

$$p\begin{bmatrix} \mathbf{q}_c \\ \mathbf{i}_x \end{bmatrix} = \begin{bmatrix} \mathbf{0} & \mathbf{M}^T\mathbf{B}_b^T \\ -\mathbf{L}_x^{-1}\mathbf{P}_x & -\mathbf{L}_x^{-1}(\mathbf{r}_x + p\mathbf{L}_x) \end{bmatrix} \begin{bmatrix} \mathbf{q}_c \\ \mathbf{i}_x \end{bmatrix} + \begin{bmatrix} \mathbf{M}^T & \mathbf{0} \\ \mathbf{0} & -\mathbf{L}_x^{-1}\mathbf{B}_b \end{bmatrix} \begin{bmatrix} \mathbf{j}_{br} \\ \mathbf{e}_{br} \end{bmatrix} \tag{3.14}$$

$$\begin{bmatrix} \mathbf{i}_{br} \\ \mathbf{v}_{br} \end{bmatrix} =$$

$$\begin{bmatrix} \mathbf{0} & \mathbf{B}_b^T \\ \mathbf{P}_{br}\mathbf{M} - \mathbf{L}_{br}\mathbf{B}_b^T\mathbf{L}_x^{-1}\mathbf{P}_x & (\mathbf{r}_{br} + p\mathbf{L}_{br})\mathbf{B}_b^T - \mathbf{L}_{br}\mathbf{B}_b^T\mathbf{L}_x^{-1}(\mathbf{r}_x + p\mathbf{L}_x) \end{bmatrix} \begin{bmatrix} \mathbf{q}_c \\ \mathbf{i}_x \end{bmatrix}$$
$$+ \begin{bmatrix} \mathbf{0} & \mathbf{0} \\ \mathbf{0} & \mathbf{I} - \mathbf{L}_{br}\mathbf{B}_b^T\mathbf{L}_x^{-1}\mathbf{B}_b \end{bmatrix} \begin{bmatrix} \mathbf{j}_{br} \\ \mathbf{e}_{br} \end{bmatrix} \tag{3.15}$$

$\mathbf{M}$ is a $b \times b$ matrix whose entries $m_{i,j} = 1$ if the j^{th} capacitor is connected to the j^{th} branch and 0 otherwise. $\mathbf{L}_x$ and $\mathbf{r}_x$ are defined in (3.16) and (3.17), respectively.

$$\mathbf{L}_x = \mathbf{B}_b\mathbf{L}_{br}\mathbf{B}_b^T \tag{3.16}$$

$$\mathbf{r}_x = \mathbf{B}_b\mathbf{r}_{br}\mathbf{B}_b^T \tag{3.17}$$

The state vector $\begin{bmatrix} \mathbf{q}_c & \mathbf{i}_x \end{bmatrix}^T$ will have $2(b - n + 1)$ variables. If the system has no capacitance, $\mathbf{q}_c = 0$ and the system will have $b - n + 1$ states. $\mathbf{i}_{br}$, $\mathbf{v}_{br}$, $\mathbf{j}_{br}$, and $\mathbf{e}_{br}$ each have b entries so the vectors $\begin{bmatrix} \mathbf{i}_{br} & \mathbf{v}_{br} \end{bmatrix}^T$ and $\begin{bmatrix} \mathbf{j}_{br} & \mathbf{e}_{br} \end{bmatrix}^T$ are each $2b$ dimensional. Considering these established results, the state-space matrices $\mathbf{A}$, $\mathbf{B}$, $\mathbf{C}$, and $\mathbf{D}$ will be of size $(2(b - n + 1) \times 2(b - n + 1))$, $(2(b - n + 1) \times 2b)$, $(2b \times 2(b - n + 1))$, and $(2b \times 2b)$, respectively.

In (3.14) - (3.15), the output voltages of the m inverter models, $\{\mathbf{e}_{\text{inv1}(abc)}, \ldots, \mathbf{e}_{\text{inv}m(abc)}\}$, and the infinite bus voltages, $\mathbf{e}_{\infty(abc)}$, constitute the non-zero entries in the voltage-source vector $\mathbf{e}_{br}$ for their associated branch indices. The non-linear state-equations of each inverter model are implemented graphically outside the ASMG model using Simulink. Because the microgrid model has no current sources, $\mathbf{j}_{br} = \mathbf{0}$ and the non-zero elements of the input vector $\mathbf{u}$ are exclusively voltage sources.

3.4 Summary

After calculating the transformer parameters as outlined in Section 3.1 and numbering the system branches and nodes, the system can be represented

using a state-space model. The information describing the structure of the microgrid is contained in $\mathbf{A}_a$ and the system parameters are summarized in the matrices $\mathbf{r}_{br}$, $\mathbf{L}_{br}$, and $\mathbf{P}_{br}$. The infinite bus voltages and the inverter output voltages form the non-zero entries in the input voltage source vector $\mathbf{e}_{br}$ and there are no current sources. The microgrid model is complete and can be used to model the system response to both large and small disturbances.

CHAPTER 4

SMALL-SIGNAL MODEL DEVELOPMENT

The presented method is used to derive a linearized model of a microgrid. Once complete, small-signal stability can be analyzed with respect to any system parameter. For the derivation shown to be valid, the three-phase system must have no transformers and branch numberings cannot be arbitrary.

4.1 Transformed State-Space Model

The system state equations expressed in the *abc* frame in (3.14) and (3.15) are time-varying in steady state. Therefore, Park's transformation is used to transform them to $qd0$ variables so that the equilibrium values are steady-state quantities. Park's transformation, as defined in (4.1), can be used to transform a set of three-phase variables, $\mathbf{f}_{abc(1)}$, to $qd0$ quantities using (4.2).

$$\mathbf{K}_s = \frac{2}{3}\begin{bmatrix} \cos\theta & \cos\left(\theta - \frac{2\pi}{3}\right) & \cos(\theta + \frac{2\pi}{3}) \\ \sin\theta & \sin\left(\theta - \frac{2\pi}{3}\right) & \sin(\theta + \frac{2\pi}{3}) \\ \frac{1}{2} & \frac{1}{2} & \frac{1}{2} \end{bmatrix} \tag{4.1}$$

$$\mathbf{f}_{qd0(1)} = \mathbf{K}_s \mathbf{f}_{abc(1)} \tag{4.2}$$

The angle θ represents the position of the arbitrary reference frame and can be expressed using (4.3), where ω is the reference frame speed and θ_0 is the initial position [29].

$$\theta = \int \omega \, dt + \theta_0 \tag{4.3}$$

To transform N groups of three-phase variables, the matrix $\mathbf{\Gamma}$ and its inverse are defined as

$$\mathbf{\Gamma} = \begin{bmatrix} \mathbf{K}_s & \mathbf{0}_{(3\times3)} & \dots & \mathbf{0}_{(3\times3)} \\ \mathbf{0}_{(3\times3)} & \mathbf{K}_s & \dots & \mathbf{0}_{(3\times3)} \\ \vdots & \vdots & \ddots & \vdots \\ \mathbf{0}_{(3\times3)} & \mathbf{0}_{(3\times3)} & \dots & \mathbf{K}_s \end{bmatrix}_{(3N\times3N)} \tag{4.4}$$

and

$$\mathbf{\Gamma}^{-1} = \begin{bmatrix} \mathbf{K}_s^{-1} & \mathbf{0}_{(3\times3)} & \dots & \mathbf{0}_{(3\times3)} \\ \mathbf{0}_{(3\times3)} & \mathbf{K}_s^{-1} & \dots & \mathbf{0}_{(3\times3)} \\ \vdots & \vdots & \ddots & \vdots \\ \mathbf{0}_{(3\times3)} & \mathbf{0}_{(3\times3)} & \dots & \mathbf{K}_s^{-1} \end{bmatrix}_{(3N\times3N)} \tag{4.5}$$

Applying the transformation $\mathbf{\Gamma}$ to a vector containing N collections of three-phase variables gives

$$\begin{bmatrix} \mathbf{f}_{qdo(1)} \\ \mathbf{f}_{qdo(2)} \\ \vdots \\ \mathbf{f}_{qdo(N)} \end{bmatrix} = \mathbf{\Gamma} \begin{bmatrix} \mathbf{f}_{abc(1)} \\ \mathbf{f}_{abc(2)} \\ \vdots \\ \mathbf{f}_{abc(N)} \end{bmatrix} \tag{4.6}$$

The small-signal microgrid model will be developed for static topologies so that the node-incidence matrix, $\mathbf{A}_a$, is time invariant. Additionally, the parameter matrices $\mathbf{r}_{br}$, $\mathbf{L}_{br}$, and $\mathbf{P}_{br}$ are constant valued. Thus, the resulting state-space matrix coefficients $\mathbf{A}$, $\mathbf{B}$, $\mathbf{C}$, and $\mathbf{D}$ will also have no time dependence since they are derived from $\mathbf{A}_a$, $\mathbf{r}_{br}$, $\mathbf{L}_{br}$, and $\mathbf{P}_{br}$. In order to use (4.6), the branches must be numbered so that the vectors $\mathbf{y} = \begin{bmatrix} \mathbf{i}_{br} & \mathbf{v}_{br} \end{bmatrix}^T$ and $\mathbf{u} = \begin{bmatrix} \mathbf{j}_{br} & \mathbf{e}_{br} \end{bmatrix}^T$ take the general form

$$\mathbf{F}_{abc} = \begin{bmatrix} \mathbf{F}_{abc(1)} \\ \mathbf{F}_{abc(2)} \\ \vdots \\ \mathbf{F}_{abc(N)} \end{bmatrix} = \begin{bmatrix} f_{a(1)}(t) \\ f_{b(1)}(t) \\ f_{c(1)}(t) \\ \vdots \\ f_{a(N)}(t) \\ f_{b(N)}(t) \\ f_{c(N)}(t) \end{bmatrix} \tag{4.7}$$

Similarly, the state vector $\mathbf{x} = \begin{bmatrix} \mathbf{q}_c & \mathbf{i}_x \end{bmatrix}^T$ also takes the form shown in (4.7). The state variable, input, and output vectors are are transformed so that

$$\left\{ \begin{array}{l} \mathbf{x}_{qd0} = \mathbf{\Gamma}\mathbf{x}_{abc} \\ \mathbf{u}_{qd0} = \mathbf{\Gamma}\mathbf{u}_{abc} \\ \mathbf{y}_{qd0} = \mathbf{\Gamma}\mathbf{y}_{abc} \end{array} \right\} \tag{4.8}$$

and consequently

$$\left\{ \begin{array}{l} \mathbf{x}_{abc} = \mathbf{\Gamma}^{-1}\mathbf{x}_{qd0} \\ \mathbf{u}_{abc} = \mathbf{\Gamma}^{-1}\mathbf{u}_{qd0} \\ \mathbf{y}_{abc} = \mathbf{\Gamma}^{-1}\mathbf{y}_{qd0} \end{array} \right\} \tag{4.9}$$

The derivative term in the state-space model can now be expressed using the product rule [29].

$$p\mathbf{x}_{abc} = p(\mathbf{\Gamma}^{-1}\mathbf{x}_{qd0}) = p(\mathbf{\Gamma}^{-1})\mathbf{x}_{qd0} + \mathbf{\Gamma}^{-1}p(\mathbf{x}_{qd0}) \tag{4.10}$$

Substituting previous results into the equation $p\mathbf{x}_{abc} = \mathbf{A}\mathbf{x}_{abc} + \mathbf{B}\mathbf{u}_{abc}$ and $\mathbf{y}_{abc} = \mathbf{C}\mathbf{x}_{abc} + \mathbf{D}\mathbf{u}_{abc}$ yields

$$p(\mathbf{\Gamma}^{-1})\mathbf{x}_{qd0} + \mathbf{\Gamma}^{-1}p(\mathbf{x}_{qd0}) = \mathbf{A}\mathbf{\Gamma}^{-1}\mathbf{x}_{qd0} + \mathbf{B}\mathbf{\Gamma}^{-1}\mathbf{u}_{qd0} \tag{4.11}$$

and

$$\mathbf{\Gamma}^{-1}(\mathbf{y}_{qd0}) = \mathbf{C}\mathbf{\Gamma}^{-1}\mathbf{x}_{qd0} + \mathbf{D}\mathbf{\Gamma}^{-1}\mathbf{u}_{qd0} \tag{4.12}$$

Solving for $p(\mathbf{x}_{qd0})$ and $(\mathbf{y}_{qd0})$ in (4.11) and (4.12) gives the state-space model shown in (4.13) - (4.14).

$$p\mathbf{x}_{qd0} = (-\mathbf{\Gamma}p\mathbf{\Gamma}^{-1} + \mathbf{\Gamma}\mathbf{A}\mathbf{\Gamma}^{-1})\mathbf{x}_{qd0} + \mathbf{\Gamma}\mathbf{B}\mathbf{\Gamma}^{-1}\mathbf{u}_{qd0} \tag{4.13}$$

$$\mathbf{y}_{qd0} = \mathbf{\Gamma}\mathbf{C}\mathbf{\Gamma}^{-1}\mathbf{x}_{qd0} + \mathbf{\Gamma}\mathbf{D}\mathbf{\Gamma}^{-1}\mathbf{u}_{qd0} \tag{4.14}$$

The presented state-space model can be simplified further. It can be shown that $\mathbf{K}_s p \mathbf{K}_s^{-1}$ reduces to the constant valued matrix in (4.15) [29].

$$\mathbf{K}_s p \mathbf{K}_s^{-1} = \omega \begin{bmatrix} 0 & 1 & 0 \\ -1 & 0 & 0 \\ 0 & 0 & 0 \end{bmatrix} \tag{4.15}$$

Thus, $-\mathbf{\Gamma} p \mathbf{\Gamma}^{-1}$ becomes a constant matrix with expression (4.15) filling in the entries along each 3×3 block-diagonal element and zeros everywhere else. Additionally, if there exists a 3×3 symmetric matrix, $\mathbf{S}$, of the form

$$\mathbf{S} = \begin{bmatrix} L & M & M \\ M & L & M \\ M & M & L \end{bmatrix} \tag{4.16}$$

then the expression $\mathbf{K}_s \mathbf{S} \mathbf{K}_s^{-1}$ reduces to a diagonal matrix $\mathbf{D}$ in (4.17) [29].

$$\mathbf{K}_s \mathbf{S} \mathbf{K}_s^{-1} = \begin{bmatrix} L & 0 & 0 \\ 0 & L & 0 \\ 0 & 0 & L \end{bmatrix} = \mathbf{D} \tag{4.17}$$

Therefore, because the aforementioned branch numbering requirement described in (4.7) ensures that the matrix $\mathbf{A}$ is of the form

$$\mathbf{A} = \begin{bmatrix} \mathbf{S}_{(1,1)} & \mathbf{S}_{(1,2)} & \dots & \mathbf{S}_{(1,n)} \\ \mathbf{S}_{(2,1)} & \mathbf{S}_{(2,2)} & \dots & \mathbf{S}_{(2,n)} \\ \vdots & \vdots & \ddots & \vdots \\ \mathbf{S}_{(n,1)} & \mathbf{S}_{(n,2)} & \dots & \mathbf{S}_{(n,n)} \end{bmatrix} \tag{4.18}$$

then the matrix coefficient $\mathbf{\Gamma A \Gamma}^{-1}$ in (4.13) becomes the constant-valued matrix in (4.19)

$$\mathbf{\Gamma A \Gamma}^{-1} = \begin{bmatrix} \mathbf{D}_{(1,1)} & \mathbf{D}_{(1,2)} & \dots & \mathbf{D}_{(1,n)} \\ \mathbf{D}_{(2,1)} & \mathbf{D}_{(2,2)} & \dots & \mathbf{D}_{(2,n)} \\ \vdots & \vdots & \ddots & \vdots \\ \mathbf{D}_{(n,1)} & \mathbf{D}_{(n,2)} & \dots & \mathbf{D}_{(n,n)} \end{bmatrix} \tag{4.19}$$

By similar arguments, it can be shown that for the transformed state-space model in (4.13) - (4.14), every matrix coefficient is time invariant and the matrices $\mathbf{\Gamma B \Gamma}^{-1}$, $\mathbf{\Gamma C \Gamma}^{-1}$, and $\mathbf{\Gamma D \Gamma}^{-1}$ are also of the form in (4.19).

Given a balanced set of three-phase *abc* voltages

$$\mathbf{V}_{abc} = |V_{\text{pk}}| \begin{bmatrix} \cos(\theta_v(t)) \\ \cos(\theta_v(t) - \frac{2\pi}{3}) \\ \cos(\theta_v(t) + \frac{2\pi}{3}) \end{bmatrix} \tag{4.20}$$

the transformation into the arbitrary reference frame with position θ yields (4.21) [29].

$$\mathbf{V}_{qd0} = |V_{\text{pk}}| \begin{bmatrix} \cos(\theta_v(t) - \theta) \\ -\sin(\theta_v(t) + \theta) \\ 0 \end{bmatrix} \tag{4.21}$$

For the microgrid state-space model, the non-zero elements in the input vector $\mathbf{e}_{br}$ are composed of the balanced inverter voltages

$$\mathbf{e}_{\text{inv}(abc)} = \left(z + K_p \left(\frac{QM_q}{S_{\text{base}}} + E^* - \frac{V}{V_{\text{base}}} \right) \right) \begin{bmatrix} \cos(\theta_v(t)) \\ \cos(\theta_v(t) - \frac{2\pi}{3}) \\ \cos(\theta_v(t) + \frac{2\pi}{3}) \end{bmatrix} \tag{4.22}$$

and the infinite bus voltages

$$\mathbf{e}_{\infty(abc)} = |V_{\text{pk(LN)}}| \begin{bmatrix} \cos(\omega_0 t) \\ \cos(\omega_0 t - \frac{2\pi}{3}) \\ \cos(\omega_0 t + \frac{2\pi}{3}) \end{bmatrix} \tag{4.23}$$

By choosing the synchronous reference frame so that $\theta = \omega_0 t$, the transformed inverter voltages and infinite-bus voltages become

$$\mathbf{e}_{\text{inv}(qd0)} = \left(z + K_p \left(\frac{QM_q}{S_{\text{base}}} + E^* - \frac{V}{V_{\text{base}}} \right) \right) \begin{bmatrix} \cos(\theta_v(t) - \omega_0 t) \\ -\sin(\theta_v(t) + \omega_0 t) \\ 0 \end{bmatrix} \tag{4.24}$$

and

$$\mathbf{e}_{\infty(qd0)} = \begin{bmatrix} |V_{\text{pk(LN)}}| \\ 0 \\ 0 \end{bmatrix} \tag{4.25}$$

The vector $\mathbf{e}_{\infty(qd0)}$ will always remain constant valued and the entries in

(4.24) will approach a constant steady-state.

4.2 Closed-Loop Equations

Before the system can be linearized for stability analysis, the closed-loop state equations must be expressed. In this context, the ASMG state-space model represents the plant and the inverter state equations of Chapter 2 form the feedback equations. The closed-loop state-equations of the system will be expressed in the form

$$p\bar{\mathbf{x}} = \mathbf{f}(\bar{\mathbf{x}}) \tag{4.26}$$

where $\mathbf{f}(\bar{\mathbf{x}})$ is non-linear and $\bar{\mathbf{x}}$ contains both the inverter control and ASMG state-variables, $\mathbf{x}_{\text{inv}}$ and $\mathbf{x}_{qd0}$, respectively. $\bar{\mathbf{x}}$ may be written as

$$\bar{\mathbf{x}} = \begin{bmatrix} \mathbf{x}_{qd0} \\ \mathbf{x}_{\text{inv}} \end{bmatrix} \tag{4.27}$$

The state vector $\mathbf{x}_{qd0}$ contains N collections of three-phase state-variables so that $\mathbf{x}_{qd0}$ is $3N$ dimensional and is of the form

$$\mathbf{x}_{qd0} = \begin{bmatrix} \mathbf{x}_{qd0(1)} \\ \mathbf{x}_{qd0(2)} \\ \vdots \\ \mathbf{x}_{qd0(N)} \end{bmatrix} = \begin{bmatrix} x_{q(1)} \\ x_{d(1)} \\ x_{0(1)} \\ \vdots \\ x_{q(N)} \\ x_{d(N)} \\ x_{0(N)} \end{bmatrix} \tag{4.28}$$

and for a system with m microsource inverters, $\mathbf{x}_{\text{inv}}$ is a $5m$ dimensional vector composed of inverter state variables as shown in (4.29).

$$\mathbf{x}_{\text{inv}} = \begin{bmatrix} \mathbf{x}_{\text{inv}(1)} \\ \vdots \\ \mathbf{x}_{\text{inv}(m)} \end{bmatrix} = \begin{bmatrix} \theta_{v(1)} \\ z_{(1)} \\ P_{(1)} \\ Q_{(1)} \\ V_{(1)} \\ \vdots \\ \theta_{v(m)} \\ z_{(m)} \\ P_{(m)} \\ Q_{(m)} \\ V_{(m)} \end{bmatrix} \tag{4.29}$$

For concreteness, the sample system in Figure 4.1 will be considered. This system is composed of six branches and four nodes. Since there is no capacitance, only currents will be state-variables. Using (4.13) and (4.14), the transformed state-space model for this particular system is shown in (4.30) and (4.31).

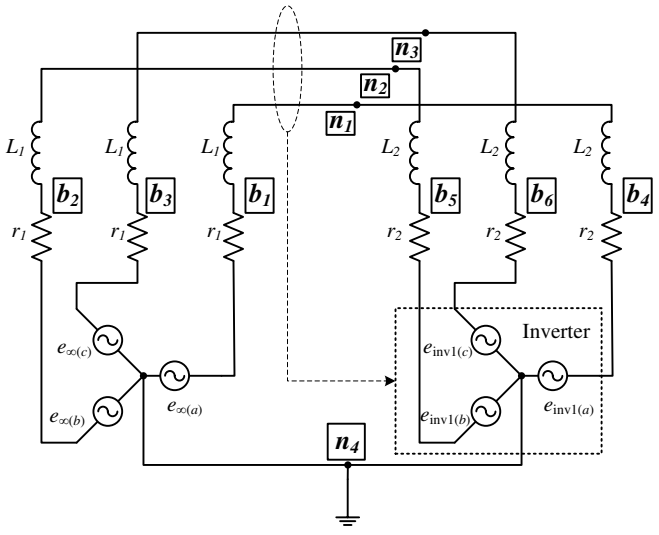

Figure 4.1: Example three-phase power system containing one inverter and infinite bus

$$p\left[\mathbf{i}_{qd0(2)}\right] = \hat{a}_{11}\left[\mathbf{I}\right]\left[\mathbf{i}_{qd0(2)}\right] + \begin{bmatrix} \hat{b}_{11}\mathbf{I} & \hat{b}_{12}\mathbf{I} \end{bmatrix} \begin{bmatrix} \mathbf{e}_{\infty(qd0)} \\ \mathbf{e}_{\text{inv}(qd0)} \end{bmatrix} \tag{4.30}$$

$$\begin{bmatrix} \mathbf{i}_{qd0(1)} \\ \mathbf{i}_{qd0(2)} \\ \mathbf{v}_{qd0(1)} \\ \mathbf{v}_{qd0(2)} \end{bmatrix} = \begin{bmatrix} \hat{c}_{11}\mathbf{I} \\ \hat{c}_{21}\mathbf{I} \\ \hat{c}_{31}\mathbf{I} \\ \hat{c}_{41}\mathbf{I} \end{bmatrix} \begin{bmatrix} \mathbf{i}_{qd0(2)} \end{bmatrix} + \begin{bmatrix} \hat{d}_{11}\mathbf{I} & \hat{d}_{12}\mathbf{I} \\ \hat{d}_{21}\mathbf{I} & \hat{d}_{22}\mathbf{I} \\ \hat{d}_{31}\mathbf{I} & \hat{d}_{32}\mathbf{I} \\ \hat{d}_{41}\mathbf{I} & \hat{d}_{42}\mathbf{I} \end{bmatrix} \begin{bmatrix} \mathbf{e}_{\infty(qd0)} \\ \mathbf{e}_{\text{inv}(qd0)} \end{bmatrix} \tag{4.31}$$

where each $\mathbf{I}$ is a 3×3 identity matrix. The inverter state-variable vector is

$$\mathbf{x}_{\text{inv}} = \begin{bmatrix} \mathbf{x}_{\text{inv}(1)} \end{bmatrix} = \begin{bmatrix} \theta_{v(1)} \\ z_{(1)} \\ P_{(1)} \\ Q_{(1)} \\ V_{(1)} \end{bmatrix} \tag{4.32}$$

Before the system-level equations may be put into the form of (4.26), it is necessary to outline the algebraic relationships needed.

It has been shown that by using (4.24) and (4.25), the infinite bus voltages, $\mathbf{e}_{\infty(qd0)}$, reduce to constants and the inverter voltages, $\mathbf{e}_{\text{inv}(qd0)}$, may be expressed in terms of the inverter control state-variables. Since there are no current sources, the non-zero elements of the total input vector $\mathbf{u}_{qd0}$ are composed of the voltage source equations $\mathbf{e}_{\text{inv}(qd0)}$ and $\mathbf{e}_{\infty(qd0)}$. After substituting the voltage source expressions (4.24) and (4.25) into the input vector, $\mathbf{u}_{qd0}$ can be written in terms of the inverter state variables as illustrated in (4.33).

$$\mathbf{u}_{qd0} = \mathbf{g}_{\alpha}(\mathbf{x}_{\text{inv}}) \tag{4.33}$$

In the case of the sample system, $\mathbf{u}_{qd0}$ becomes

$$\mathbf{u}_{qd0} = \begin{bmatrix} \mathbf{e}_{\infty(qd0)} \\ \mathbf{e}_{\text{inv}(qd0)} \end{bmatrix} = \mathbf{g}_{\alpha}(\mathbf{x}_{\text{inv}}) = \begin{bmatrix} |V_{\text{pk(LN)}}| \\ 0 \\ 0 \\ \left(z + K_p\left(\frac{QM_q}{S_{\text{base}}} + E^* - \frac{V}{V_{\text{base}}}\right)\right)\cos(\theta_v(t) - \omega_0 t) \\ -\left(z + K_p\left(\frac{QM_q}{S_{\text{base}}} + E^* - \frac{V}{V_{\text{base}}}\right)\right)\sin(\theta_v(t) + \omega_0 t) \\ 0 \end{bmatrix} \tag{4.34}$$

Thus, the ASMG state equation in (4.13) can be expressed in terms of $\mathbf{x}_{qd0}$ and $\mathbf{x}_{\text{inv}}$ as shown in (4.35), where $\mathbf{A}' = -\mathbf{\Gamma} p \mathbf{\Gamma}^{-1} + \mathbf{\Gamma A \Gamma}^{-1}$.

$$p\mathbf{x}_{qd0} = \mathbf{A}'\mathbf{x}_{qd0} + \mathbf{\Gamma B \Gamma}^{-1}\mathbf{u}_{qd0} = \mathbf{A}'\mathbf{x}_{qd0} + \mathbf{\Gamma B \Gamma}^{-1}\mathbf{g}_{\alpha}(\mathbf{x}_{\text{inv}}) = \mathbf{G}(\mathbf{x}_{qd0}, \mathbf{x}_{\text{inv}}) = \mathbf{G}(\bar{\mathbf{x}}) \tag{4.35}$$

Since the ASMG state-equations in (4.35) are in terms of state variables, all that is left is to express the inverter state-equations in terms of $\bar{\mathbf{x}}$. Once that is complete, the results can be combined with (4.35) to create the final form shown in (4.26).

As described in Chapter 2, the state-equations for each microsource inverter are

$$pP = \frac{\tilde{P} - P}{\tau_P} \tag{4.36}$$

$$pQ = \frac{\tilde{Q} - Q}{\tau_Q} \tag{4.37}$$

$$pV = \frac{\tilde{V} - V}{\tau_V} \tag{4.38}$$

$$p\theta_v = M_p(P^* - P) \tag{4.39}$$

$$pz = K_i \left(\frac{QM_q}{S_{\text{base}}} + E^* - \frac{V}{V_{\text{base}}} \right) \tag{4.40}$$

Since (4.39) and (4.40) are already written in terms of states, only (4.36) - (4.38) must be manipulated to reach the desired form. Recalling that the unfiltered values $\tilde{P}$, $\tilde{Q}$, and $\tilde{V}$ appearing in (4.36) - (4.38) are defined as

$$\tilde{P} = \frac{3}{2}(V_d I_d + V_q I_q + 2V_0 I_0) \tag{4.41}$$

$$\tilde{Q} = \frac{3}{2}(V_d I_q - V_q I_d) \tag{4.42}$$

$$\tilde{V} = \sqrt{V_d^2 + V_q^2} \tag{4.43}$$

it is necessary to express the voltages and currents appearing in (4.41) - (4.43) in terms of the system state-variables. Recalling that $\mathbf{y}_{qd0}$ is defined as

$$\mathbf{y}_{qd0} = \begin{bmatrix} \mathbf{i}_{br(qd0)} \\ \mathbf{v}_{br(qd0)} \end{bmatrix} \tag{4.44}$$

the equation containing the system voltages and currents, $\mathbf{y}_{qd0} = \mathbf{\Gamma C \Gamma}^{-1}\mathbf{x}_{qd0} + \mathbf{\Gamma D \Gamma}^{-1}\mathbf{u}_{qd0}$, can be written in terms of the states after making the substitution $\mathbf{u}_{qd0} = \mathbf{g}_{\alpha}(\mathbf{x}_{\text{inv}})$. The function $\mathbf{h}(\bar{\mathbf{x}})$ is a vector containing non-linear functions of the system states.

$$\begin{bmatrix} \mathbf{i}_{br(qd0)} \\ \mathbf{v}_{br(qd0)} \end{bmatrix} = \mathbf{\Gamma C \Gamma}^{-1}\mathbf{x}_{qd0} + \mathbf{\Gamma D \Gamma}^{-1}\mathbf{g}_{\alpha}(\mathbf{x}_{\text{inv}}) = \mathbf{h}(\mathbf{x}_{qd0}, \mathbf{x}_{\text{inv}}) = \mathbf{h}(\bar{\mathbf{x}}) \tag{4.45}$$

Using (4.45), any voltage and current in (4.36) - (4.38), which appear via (4.41) - (4.43), can be expressed in terms of the states. For the sample system, (4.45) becomes

$$\begin{bmatrix} \mathbf{i}_{qd0(1)} \\ \mathbf{i}_{qd0(2)} \\ \mathbf{v}_{qd0(1)} \\ \mathbf{v}_{qd0(2)} \end{bmatrix} = \begin{bmatrix} \hat{c}_{11}\mathbf{I} \\ \hat{c}_{21}\mathbf{I} \\ \hat{c}_{31}\mathbf{I} \\ \hat{c}_{41}\mathbf{I} \end{bmatrix} \begin{bmatrix} \mathbf{i}_{qd0(2)} \end{bmatrix} + \begin{bmatrix} \hat{d}_{11}\mathbf{I} & \hat{d}_{12}\mathbf{I} \\ \hat{d}_{21}\mathbf{I} & \hat{d}_{22}\mathbf{I} \\ \hat{d}_{31}\mathbf{I} & \hat{d}_{32}\mathbf{I} \\ \hat{d}_{41}\mathbf{I} & \hat{d}_{42}\mathbf{I} \end{bmatrix} \begin{bmatrix} |V_{\text{pk(LN)}}| \\ 0 \\ 0 \\ \left(z + K_p\left(\frac{QM_q}{S_{\text{base}}} + E^* - \frac{V}{V_{\text{base}}}\right)\right)\cos(\theta_v(t) - \omega_0 t) \\ -\left(z + K_p\left(\frac{QM_q}{S_{\text{base}}} + E^* - \frac{V}{V_{\text{base}}}\right)\right)\sin(\theta_v(t) + \omega_0 t) \\ 0 \end{bmatrix} \tag{4.46}$$

After carrying out the matrix multiplications, the right-side of (4.46) can be written as a 12-row vector containing functions of state-variables as illustrated in (4.45). Using these results, any voltage and current can be expressed using states.

After making the necessary substitutions, the inverter state-equations in (4.36) - (4.40) are written in terms of the system states, $\bar{\mathbf{x}}$. In general, the combined state-equations for m inverters are written as

$$p\mathbf{x}_{\text{inv}} = \mathbf{B}(\mathbf{x}_{qd0}, \mathbf{x}_{\text{inv}}) = \mathbf{B}(\bar{\mathbf{x}}) \tag{4.47}$$

where $\mathbf{B}(\bar{\mathbf{x}})$ is a non-linear function. For the sample system

$$p\mathbf{x}_{\text{inv}} = p\begin{bmatrix} \mathbf{i}_{qd0(1)} \\ \mathbf{i}_{qd0(2)} \\ \mathbf{v}_{qd0(1)} \\ \mathbf{v}_{qd0(2)} \\ \theta_{v(1)} \\ z_{(1)} \\ P_{(1)} \\ Q_{(1)} \\ V_{(1)} \end{bmatrix} = \mathbf{B}(\mathbf{i}_{qd0(2)}, \theta_{v(1)}, z_{(1)}, P_{(1)}, Q_{(1)}, V_{(1)}) = \mathbf{B}(\bar{\mathbf{x}}) \tag{4.48}$$

Combining the ASMG and inverter control state-equations gives the final form

$$p\begin{bmatrix} \mathbf{x}_{qd0} \\ \mathbf{x}_{\text{inv}} \end{bmatrix} = p\bar{\mathbf{x}} = \begin{bmatrix} \mathbf{G}(\mathbf{x}_{qd0}, \mathbf{x}_{\text{inv}}) \\ \mathbf{B}(\mathbf{x}_{qd0}, \mathbf{x}_{\text{inv}}) \end{bmatrix} = \mathbf{f}(\bar{\mathbf{x}}) \tag{4.49}$$

4.3 Linearization

There are $3N$ and $5m$ state variables in the vectors $\mathbf{x}_{qd0}$ and $\mathbf{x}_{\text{inv}}$, respectively. However, the zero-axis equations may be omitted if the system remains balanced during small-disturbances and the number of state variables will be reduced to $2N + 5m$. The final expression is non-linear and must be linearized before eigenvalues can be evaluated. Evaluating the Jacobian of $\mathbf{f}(\bar{\mathbf{x}})$ at the equilibrium, $\bar{\mathbf{x}}_0$, and setting the zero-axis variables to zero gives the $(2N + 5m) \times (2N + 5m)$ matrix $\mathbf{L}$ in (4.50).

$$\mathbf{L} = \left[\begin{array}{cccc} \frac{\partial f_1}{\partial \bar{x}_1} & \frac{\partial f_1}{\partial \bar{x}_2} & \cdots & \frac{\partial f_1}{\partial \bar{x}_{2n+5m}} \\ \frac{\partial f_2}{\partial \bar{x}_1} & \frac{\partial f_2}{\partial \bar{x}_2} & \cdots & \frac{\partial f_2}{\partial \bar{x}_{2n+5m}} \\ \vdots & \vdots & \ddots & \vdots \\ \frac{\partial f_{2n+5m}}{\partial \bar{x}_1} & \frac{\partial f_{2n+5m}}{\partial \bar{x}_2} & \cdots & \frac{\partial f_{2n+5m}}{\partial \bar{x}_{2n+5m}} \end{array} \right] \Bigg|_{\bar{\mathbf{x}}=\bar{\mathbf{x}}_0} \tag{4.50}$$

Since it may be impractical and difficult to analytically obtain the equilibrium values, $\bar{\mathbf{x}}_0$, the steady-state values of the transformed state-space model in (4.13) - (4.14) may be used. The linearized closed-loop model of the microgrid system is shown in (4.51).

$$p\delta\bar{\mathbf{x}} = \mathbf{L}\delta\bar{\mathbf{x}} \tag{4.51}$$

4.4 Summary

Using (4.51), the stability of the microgrid may be analyzed with respect to the inverter control parameters M_p, M_q, K_p, and K_i. Small-signal system stability is maintained as long as the eigenvalues of $\mathbf{L}$ are in the left-hand side of the complex-plane. After performing small perturbations on each control parameter while analyzing the eigenvalue locations, the relationship between the inverter control control gains and system stability can be analyzed with a root-locus plot. Using this method, stability can also be evaluated with respect to load resistances, grid-utility frequency and voltage, inverter output inductance, and almost any other system parameter.

CHAPTER 5

CASE STUDIES

5.1 Large-Transient Simulation

The microgrid system shown in Figure 5.1, with parameters summarized in Appendix A, has been verified experimentally in [30]. Here, this physical system is used to verify the large signal transient model introduced in Chapter 3. The loads, rated to consume a total of 18 kW, are purely resistive and connected in floating-star configurations. The two microsources are configured for unit-power control and will regulate the measured quantities indicated in Figure 5.1.

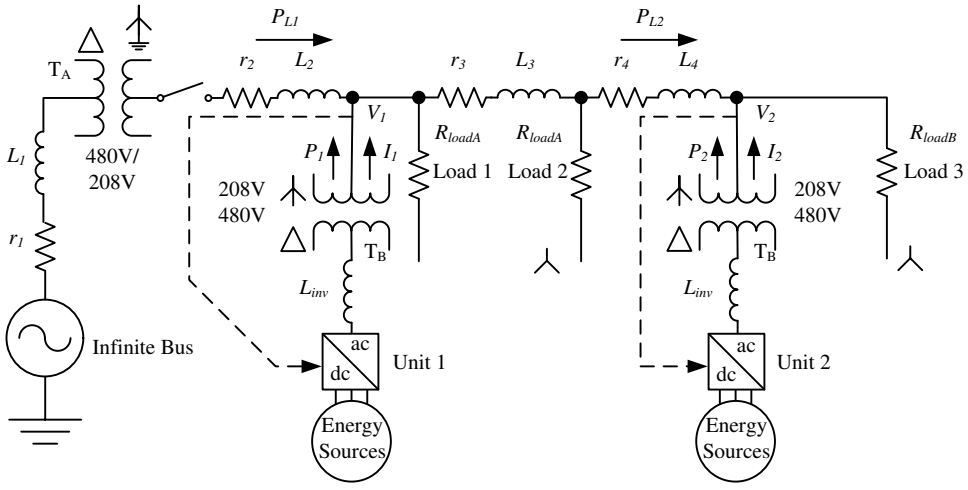

Figure 5.1: One-line diagram of dual-inverter microgrid testbed

The microgrid testbed is modeled as a circuit containing 44 branches and 24 nodes and line shunt capacitances are neglected. Since the circuit has no capacitance, the state-space model reduces to (5.1) - (5.2) and only currents are states.

$$p\left[\mathbf{i}_x\right] = \left[-\mathbf{L}_x^{-1}(\mathbf{r}_x + p\mathbf{L}_x)\right]\left[\mathbf{i}_x\right] + \left[-\mathbf{L}_x^{-1}\mathbf{B}_b\right]\left[\mathbf{e}_{br}\right] \tag{5.1}$$

$$\begin{bmatrix}\mathbf{i}_{br}\\ \mathbf{v}_{br}\end{bmatrix} = \left[(\mathbf{r}_{br} + p\mathbf{L}_{br})\mathbf{B}_b^T - \mathbf{L}_{br}\mathbf{B}_b^T\mathbf{L}_x^{-1}(\mathbf{r}_x + p\mathbf{L}_x)\right]\left[\mathbf{i}_x\right] + \left[\mathbf{I} - \mathbf{L}_{br}\mathbf{B}_b^T\mathbf{L}_x^{-1}\mathbf{B}_b\right]\left[\mathbf{e}_{br}\right] \tag{5.2}$$

There are $b - n + 1 = 21$ state variable currents. The three-phase transformers are modeled as described in Chapter 3, and the grid system is modeled as an infinite bus with an equivalent impedance $r_1 + j\omega L_1$. The two inverters are implemented using the state-equations of Section 2.2.1.

Initially, the system is connected to the utility and both microsources are regulating their power outputs, P_1 and P_2, respectively, to 0.4 pu on a 15 kW base. At t = 0.25 sec, the system is islanded and the two microsources each increase their power output to 0.6 pu to accommodate the total microgrid load 1.2 pu (18 kW). As seen in Figure 5.2, the frequency of Unit 1 decreases as its power and current output increase and steady-state operation is reached. Each phase of the islanding switch opens at current zero-crossings and the transition to islanding is complete within one cycle. Consequently, the power flow in line 1, P_{L1}, abruptly reaches zero as each phase of the three-phase switch is opened. The voltage regulated by Unit 1, V_1, is nearly constant to provide a seamless voltage during the transition.

Similar to Unit 1, the power and current output of Unit 2 increases while the frequency decreases. The regulated voltage, V_2, remains nearly constant. Both units are synchronized without communication and exhibit a unified frequency. In steady-state conditions, loads 1 and 2 are predominantly powered by Unit 1 and load 3 is almost exclusively powered by Unit 2. Thus, the power flow along line 2, P_{L2}, approaches a small value. Simulation results, shown in Figures 5.2 and 5.3, closely match measured results from [30]. These results verify the accuracy of the modeling technique and show that this particular system is stable during islanding.

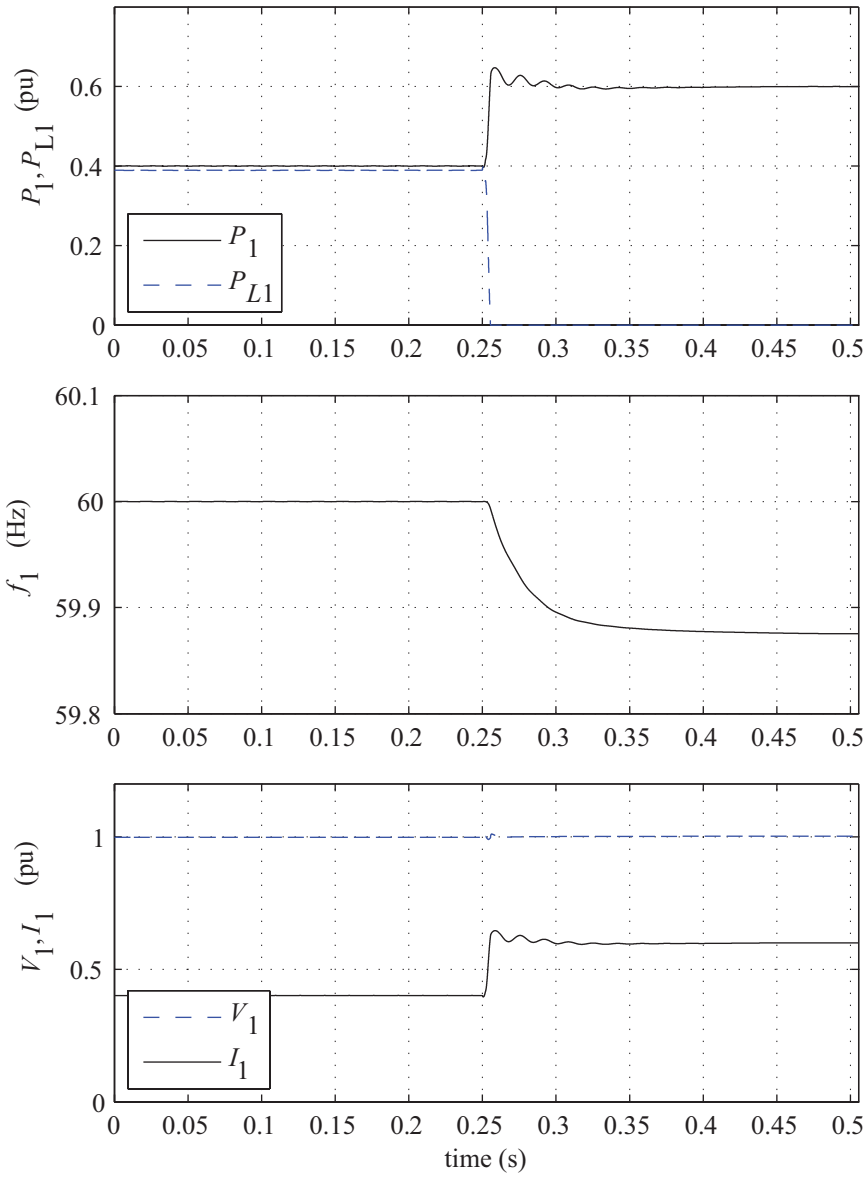

Figure 5.2: Transient response of the Unit 1 inverter and line power flow 1

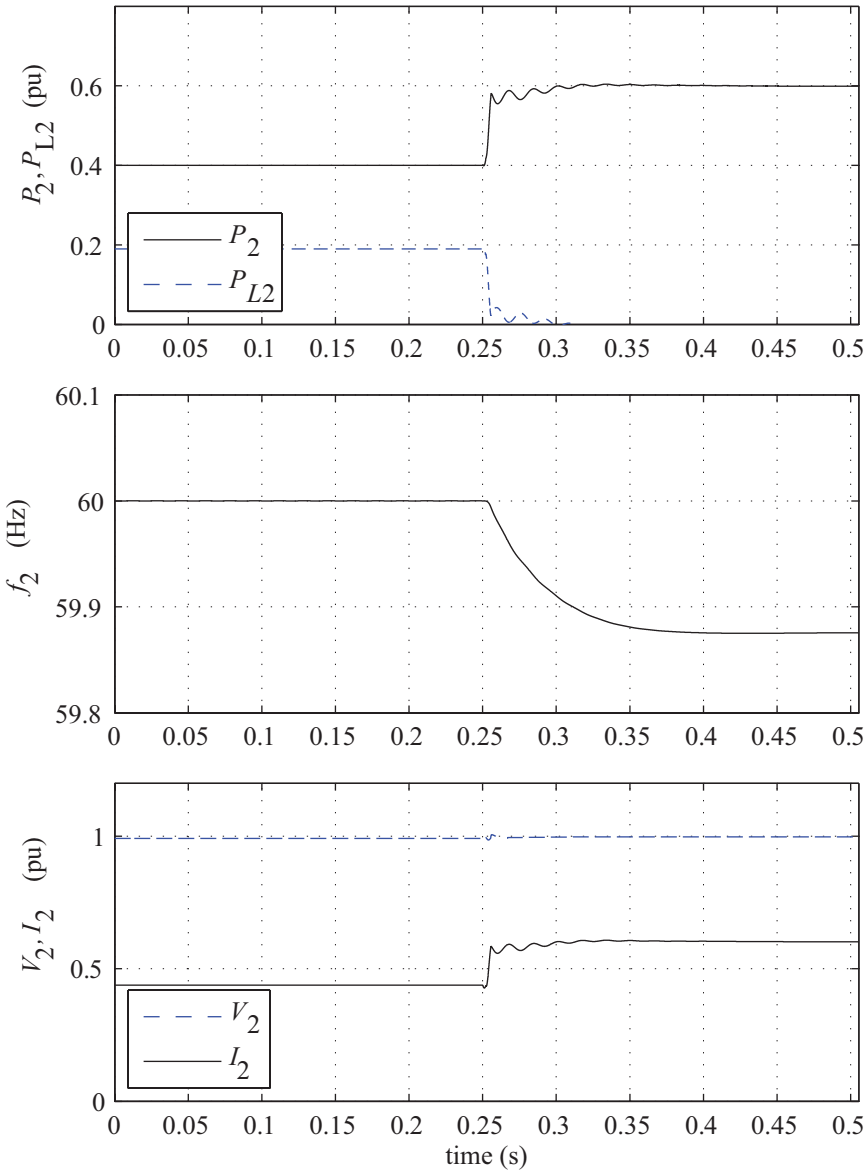

Figure 5.3: Transient response of the Unit 2 inverter and line power flow 2

5.1.1 Summary

The ASMG algorithm has been demonstrated to be effective for simulating microgrid dynamics. The presented dual-inverter microgrid was shown to be stable after the transition to islanding. The accuracy of results was confirmed using the experimental measurements in [30]. The simulation method could have also been used to model the system response to faults, load changes, utility voltage fluctuations, and any other type of disturbance. This technique is not limited to small-signal analysis and can be used to provide high resolution simulations of microgrids.

5.2 Stability Analysis

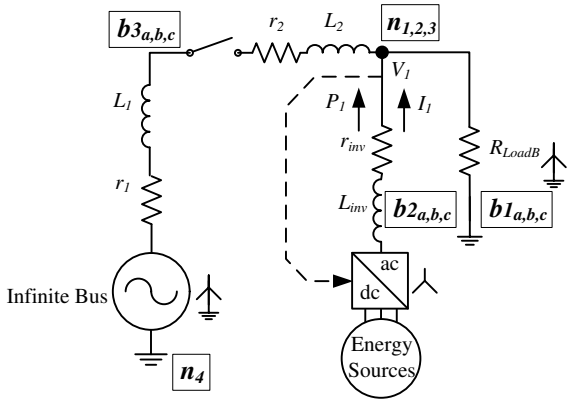

Figure 5.4: One-line diagram of three-phase single-inverter system

As indicated in Figure 5.4, this particular three-phase microgrid with no transformers can be modeled as 9 branches and 4 nodes. The stability of the system will be analyzed while the system is grid-connected. The composite branches b_{3a}, b_{3b}, and b_{3c} are formed by summing the series resistances and inductances, $r_1 + r_2$ and $L_1 + L_2$, respectively, for each phase. Shunt line capacitances are neglected and the state-space model reduces to (5.1) - (5.2). Circuit parameters are summarized in Appendix A.

5.2.1 Variable transformation

There are $b - n + 1 = 6$ state currents and the state-space model of (3.14) - (3.15) becomes

$$p\begin{bmatrix}\mathbf{i}_{abc(2)}\\ \mathbf{i}_{abc(3)}\end{bmatrix} = \begin{bmatrix}\mathbf{a}_{11} & \mathbf{a}_{12}\\ \mathbf{a}_{21} & \mathbf{a}_{22}\end{bmatrix}\begin{bmatrix}\mathbf{i}_{abc(2)}\\ \mathbf{i}_{abc(3)}\end{bmatrix} + \begin{bmatrix}\mathbf{b}_{11} & \mathbf{b}_{12} & \mathbf{b}_{13}\\ \mathbf{b}_{21} & \mathbf{b}_{22} & \mathbf{b}_{23}\end{bmatrix}\begin{bmatrix}\mathbf{0}\\ \mathbf{e}_{\text{inv1}(abc)}\\ \mathbf{e}_{\infty(abc)}\end{bmatrix} \tag{5.3}$$

$$\begin{bmatrix}\mathbf{i}_{abc(1)}\\ \mathbf{i}_{abc(2)}\\ \mathbf{i}_{abc(3)}\\ \mathbf{v}_{abc(1)}\\ \mathbf{v}_{abc(2)}\\ \mathbf{v}_{abc(3)}\end{bmatrix} = \begin{bmatrix}\mathbf{c}_{11} & \mathbf{c}_{12}\\ \mathbf{c}_{21} & \mathbf{c}_{22}\\ \mathbf{c}_{31} & \mathbf{c}_{32}\\ \mathbf{c}_{41} & \mathbf{c}_{42}\\ \mathbf{c}_{51} & \mathbf{c}_{52}\\ \mathbf{c}_{61} & \mathbf{c}_{62}\end{bmatrix}\begin{bmatrix}\mathbf{i}_{abc(2)}\\ \mathbf{i}_{abc(3)}\end{bmatrix} + \begin{bmatrix}\mathbf{d}_{11} & \mathbf{d}_{12} & \mathbf{d}_{13}\\ \mathbf{d}_{21} & \mathbf{d}_{22} & \mathbf{d}_{23}\\ \mathbf{d}_{31} & \mathbf{d}_{32} & \mathbf{d}_{33}\\ \mathbf{d}_{41} & \mathbf{d}_{42} & \mathbf{d}_{43}\\ \mathbf{d}_{51} & \mathbf{d}_{52} & \mathbf{d}_{53}\\ \mathbf{d}_{61} & \mathbf{d}_{62} & \mathbf{d}_{63}\end{bmatrix}\begin{bmatrix}\mathbf{0}\\ \mathbf{e}_{\text{inv1}(abc)}\\ \mathbf{e}_{\infty(abc)}\end{bmatrix} \tag{5.4}$$

where $\mathbf{a}_{ij}$, $\mathbf{b}_{ij}$, $\mathbf{c}_{ij}$, and $\mathbf{d}_{ij}$ are 3×3 block matrices of the form

$$\mathbf{m}_{ij} = \begin{bmatrix}\hat{m}_{ij} & 0 & 0\\ 0 & \hat{m}_{ij} & 0\\ 0 & 0 & \hat{m}_{ij}\end{bmatrix} = \hat{m}_{ij}\mathbf{I}_{(3\times 3)} \tag{5.5}$$

Recalling that the transformed state-space model is

$$p\mathbf{x}_{qd0} = (-\mathbf{\Gamma}p\mathbf{\Gamma}^{-1} + \mathbf{\Gamma}\mathbf{A}\mathbf{\Gamma}^{-1})\mathbf{x}_{qd0} + \mathbf{\Gamma}\mathbf{B}\mathbf{\Gamma}^{-1}\mathbf{u}_{qd0} \tag{5.6}$$

$$\mathbf{y}_{qd0} = \mathbf{\Gamma}\mathbf{C}\mathbf{\Gamma}^{-1}\mathbf{x}_{qd0} + \mathbf{\Gamma}\mathbf{D}\mathbf{\Gamma}^{-1}\mathbf{u}_{qd0} \tag{5.7}$$

it is necessary to calculate the matrix coefficients $\mathbf{A}'$, $\mathbf{B}'$, $\mathbf{C}'$, and $\mathbf{D}'$, which are defined as

$$\mathbf{A}' = -\mathbf{\Gamma}p\mathbf{\Gamma}^{-1} + \mathbf{\Gamma}\mathbf{A}\mathbf{\Gamma}^{-1} \tag{5.8}$$

$$\mathbf{B}' = \mathbf{\Gamma}\mathbf{B}\mathbf{\Gamma}^{-1} \tag{5.9}$$

$$\mathbf{C}' = \mathbf{\Gamma}\mathbf{C}\mathbf{\Gamma}^{-1} \tag{5.10}$$

$$\mathbf{D}' = \mathbf{\Gamma}\mathbf{D}\mathbf{\Gamma}^{-1} \tag{5.11}$$

Since the 3×3 matrix entries $\mathbf{a}_{ij}$, $\mathbf{b}_{ij}$, $\mathbf{c}_{ij}$, and $\mathbf{d}_{ij}$ are of the form in (5.5), then $\mathbf{\Gamma A \Gamma}^{-1} = \mathbf{A}$, $\mathbf{\Gamma B \Gamma}^{-1} = \mathbf{B}$, $\mathbf{\Gamma C \Gamma}^{-1} = \mathbf{C}$, and $\mathbf{\Gamma D \Gamma}^{-1} = \mathbf{D}$. Therefore,

$$\mathbf{A}' = -\begin{bmatrix} \mathbf{K}_s p \mathbf{K}_s^{-1} & \mathbf{0} \\ \mathbf{0} & \mathbf{K}_s p \mathbf{K}_s^{-1} \end{bmatrix} + \begin{bmatrix} \hat{a}_{11}\mathbf{I} & \hat{a}_{12}\mathbf{I} \\ \hat{a}_{21}\mathbf{I} & \hat{a}_{22}\mathbf{I} \end{bmatrix} = \begin{bmatrix} \hat{a}_{11} & -\omega & 0 & \hat{a}_{12} & 0 & 0 \\ \omega & \hat{a}_{11} & 0 & 0 & \hat{a}_{12} & 0 \\ 0 & 0 & \hat{a}_{11} & 0 & 0 & \hat{a}_{12} \\ \hat{a}_{21} & 0 & 0 & \hat{a}_{22} & -\omega & 0 \\ 0 & \hat{a}_{21} & 0 & \omega & \hat{a}_{22} & 0 \\ 0 & 0 & \hat{a}_{21} & 0 & 0 & \hat{a}_{22} \end{bmatrix} \tag{5.12}$$

$$\mathbf{B}' = \mathbf{B} \tag{5.13}$$

$$\mathbf{C}' = \mathbf{C} \tag{5.14}$$

$$\mathbf{D}' = \mathbf{D} \tag{5.15}$$

For this particular system, $\mathbf{B}'$, $\mathbf{C}'$, and $\mathbf{D}'$ are

$$\mathbf{B}' = \mathbf{B} = \begin{bmatrix} \hat{b}_{11}\mathbf{I} & \hat{b}_{12}\mathbf{I} & \mathbf{0} \\ \hat{b}_{21}\mathbf{I} & \mathbf{0} & \hat{b}_{23}\mathbf{I} \end{bmatrix} \tag{5.16}$$

$$\mathbf{C}' = \mathbf{C} = \begin{bmatrix} -\mathbf{I} & -\mathbf{I} \\ \mathbf{I} & \mathbf{0} \\ \mathbf{0} & \mathbf{I} \\ \hat{c}_l\mathbf{I} & \hat{c}_l\mathbf{I} \\ \hat{c}_l\mathbf{I} & \hat{c}_l\mathbf{I} \\ \hat{c}_l\mathbf{I} & \hat{c}_l\mathbf{I} \end{bmatrix} \tag{5.17}$$

$$\mathbf{D}' = \mathbf{D} = \begin{bmatrix} \mathbf{0} & \mathbf{0} & \mathbf{0} \\ \mathbf{0} & \mathbf{0} & \mathbf{0} \\ \mathbf{0} & \mathbf{0} & \mathbf{0} \\ \mathbf{I} & \mathbf{0} & \mathbf{0} \\ \mathbf{I} & \mathbf{0} & \mathbf{0} \\ \mathbf{I} & \mathbf{0} & \mathbf{0} \end{bmatrix} \tag{5.18}$$

where the numerical values of the matrix coefficients can be calculated using (5.1)- (5.2).

As outlined in Section 4.1, the inverter and infinite bus voltages in the $qd0$ synchronous frame are

$$\mathbf{e}_{\text{inv1}(qd0)} = \left(z + K_p \left(\frac{Q_1 M_q}{S_{\text{base}}} + E^* - \frac{V_1}{V_{\text{base}}} \right) \right) \begin{bmatrix} \cos(\theta_{v1}(t) - \omega_0 t) \\ -\sin(\theta_{v1}(t) + \omega_0 t) \\ 0 \end{bmatrix} \tag{5.19}$$

and

$$\mathbf{e}_{\infty(qd0)} = \begin{bmatrix} |V_{\text{pk(LN)}}| \\ 0 \\ 0 \end{bmatrix} \tag{5.20}$$

5.2.2 System equations and linearization

Using the above expressions for $\mathbf{B}'$, $\mathbf{A}'$, $\mathbf{C}'$, $\mathbf{D}'$, $\mathbf{e}_{\text{inv1}(qd0)}$, and $\mathbf{e}_{\infty(qd0)}$, the ASMG state equations reduce to the form $p\mathbf{x}_{qd0} = \mathbf{G}(\mathbf{x}_{qd0}, \mathbf{x}_{\text{inv}}) = \mathbf{G}(\bar{\mathbf{x}})$ as shown in (5.21). Eliminating the 0-axis components and substituting the previous results for this particular system yields

$$p \begin{bmatrix} I_{q(2)} \\ I_{d(2)} \\ I_{3(q)} \\ I_{3(d)} \end{bmatrix} = \begin{bmatrix} -\omega_0 \hat{a}_{11} i_{q(2)} - \omega_0 i_{d(2)} - \hat{a}_{12} i_{q(3)} + \hat{b}_{12} k_1 (x_{\text{inv1}}) \\ \omega_0 i_{q(2)} - \omega_0 \hat{a}_{11} i_{d(2)} - \hat{a}_{12} i_{d(3)} - \hat{b}_{12} k_2 (x_{\text{inv1}}) \\ -\hat{a}_{21} i_{q(2)} - \omega_0 \hat{a}_{22} i_{q(3)} - \omega_0 i_{d(3)} + \hat{b}_{22} |V_{\text{pk(LN)}}| \\ -\hat{a}_{21} i_{d(2)} + \omega_0 i_{q(3)} - \omega_0 \hat{a}_{22} i_{d(3)} \end{bmatrix} \tag{5.21}$$

where

$$k_1(x_{\text{inv1}}) = \left(z + K_p \left(\frac{Q_1 M_q}{S_{\text{base}}} + E^* - \frac{V_1}{V_{\text{base}}} \right) \right) \cos(\theta_{v1}(t) - \omega_0 t) \tag{5.22}$$

$$k_2(x_{\text{inv1}}) = \left(z + K_p \left(\frac{Q_1 M_q}{S_{\text{base}}} + E^* - \frac{V_1}{V_{\text{base}}} \right) \right) \sin(\theta_{v1}(t) - \omega_0 t) \tag{5.23}$$

To complete the closed-loop state-equations, the inverter state equations must also be expressed in terms of the states. As described in Chapter 2, the differential equations of the inverter are

$$pP_1 = \frac{\tilde{P}_1 - P_1}{\tau_P} \tag{5.24}$$

$$pQ_1 = \frac{\tilde{Q}_1 - Q_1}{\tau_Q} \tag{5.25}$$

$$pV_1 = \frac{\tilde{V}_1 - V_1}{\tau_V} \tag{5.26}$$

$$p\theta_{v1} = M_p(P^* - P_1) \tag{5.27}$$

$$pz_1 = K_i \left(\frac{Q_1 M_q}{S_{\text{base}}} + E^* - \frac{V_1}{V_{\text{base}}} \right) \tag{5.28}$$

Because (5.27) - (5.28) are already in terms of the inverter states P_1, Q_1, and V_1, only (5.24) - (5.26) require manipulation. The unfiltered quantities $\tilde{P}_1$, $\tilde{Q}_1$, and $\tilde{V}_1$ under balanced conditions are

$$\tilde{P}_1 = \frac{3}{2} \left(V_{d(2)} I_{d(2)} + V_{q(2)} I_{q(2)} \right) \tag{5.29}$$

$$\tilde{Q}_1 = \frac{3}{2} \left(V_{d(2)} I_{q(2)} - V_{q(2)} I_{d(2)} \right) \tag{5.30}$$

$$\tilde{V}_1 = \sqrt{V_{d(2)}^2 + V_{q(2)}^2} \tag{5.31}$$

In (5.29) - (5.31), the quantities $V_{q(2)}$ and $V_{d(2)}$ must be written in terms of states. After substituting expressions for $\mathbf{C}'$, $\mathbf{D}'$, (5.7) may be written as

$$\begin{bmatrix} \mathbf{I}_{qd0(1)} \\ \mathbf{I}_{qd0(2)} \\ \mathbf{I}_{qd0(3)} \\ \mathbf{V}_{qd0(1)} \\ \mathbf{V}_{qd0(2)} \\ \mathbf{V}_{qd0(3)} \end{bmatrix} = \begin{bmatrix} -\mathbf{I} & -\mathbf{I} \\ \mathbf{I} & \mathbf{0} \\ \mathbf{0} & \mathbf{I} \\ \hat{c}_l\mathbf{I} & \hat{c}_l\mathbf{I} \\ \hat{c}_l\mathbf{I} & \hat{c}_l\mathbf{I} \\ \hat{c}_l\mathbf{I} & \hat{c}_l\mathbf{I} \end{bmatrix} \begin{bmatrix} \mathbf{I}_{qd0(2)} \\ \mathbf{I}_{qd0(3)} \end{bmatrix} + \begin{bmatrix} \mathbf{0} & \mathbf{0} & \mathbf{0} \\ \mathbf{0} & \mathbf{0} & \mathbf{0} \\ \mathbf{0} & \mathbf{0} & \mathbf{0} \\ \mathbf{I} & \mathbf{0} & \mathbf{0} \\ \mathbf{I} & \mathbf{0} & \mathbf{0} \\ \mathbf{I} & \mathbf{0} & \mathbf{0} \end{bmatrix} \begin{bmatrix} \mathbf{0} \\ \mathbf{e}_{\text{inv1}(qd0)} \\ \mathbf{e}_{\infty(qd0)} \end{bmatrix} \tag{5.32}$$

Using (5.32) and setting 0-axis components to zero, $V_{q(2)}$ and $V_{d(2)}$ can be written in terms of states and substituted into (5.29) - (5.31) to produce

$$\tilde{P}_1 = \hat{c}_l \frac{3}{2} \left((I_{q(2)} + I_{q(3)}) I_{d(2)} + (I_{q(2)} + I_{q(3)}) I_{q(2)} \right) \tag{5.33}$$

$$\tilde{Q}_1 = \hat{c}_l \frac{3}{2} \left((I_{d(2)} + I_{d(3)}) I_{q(2)} - (I_{q(2)} + I_{q(3)}) I_{d(2)} \right) \tag{5.34}$$

$$\tilde{V}_1 = \hat{c}_l \sqrt{(I_{q(2)} + I_{q(3)})^2 + (I_{d(2)} + I_{d(3)})^2} \tag{5.35}$$

The inverter state equations now reduce to the form $p\mathbf{x}_{\text{inv}} = \mathbf{B}(\mathbf{x}_{qd0}, \mathbf{x}_{\text{inv}})$. Combining the ASMG and inverter state equations into $p \begin{bmatrix} \mathbf{x}_{qd} & \mathbf{x}_{\text{inv}} \end{bmatrix}^T = \mathbf{f}(\mathbf{x}_{qd}, \mathbf{x}_{\text{inv}})$ gives the non-linear state equations

$$p \begin{bmatrix} I_{q(2)} \\ I_{d(2)} \\ I_{q(3)} \\ I_{d(3)} \\ \theta_{v(1)} \\ z_{(1)} \\ P_{(1)} \\ Q_{(1)} \\ V_{(1)} \end{bmatrix} = \begin{bmatrix} -\omega_0 \hat{a}_{11} i_{q(2)} - \omega_0 i_{d(2)} - \hat{a}_{12} i_{q(3)} + \hat{b}_{12} k_1(x_{\text{inv1}}) \\ \omega_0 i_{q(2)} - \omega_0 \hat{a}_{11} i_{d(2)} - \hat{a}_{12} i_{d(3)} - \hat{b}_{12} k_2(x_{\text{inv1}}) \\ -\hat{a}_{21} i_{q(2)} - \omega_0 \hat{a}_{22} i_{q(3)} - \omega_0 i_{d(3)} + \hat{b}_{22} |V_{\text{pk(LN)}}| \\ -\hat{a}_{21} i_{d(2)} + \omega_0 i_{q(3)} - \omega_0 \hat{a}_{22} i_{d(3)} \\ M_p(P^* - P_1) \\ K_i \left(\frac{Q_1 M_q}{S_{\text{base}}} + E^* - \frac{V_1}{V_{\text{base}}} \right) \\ \frac{1}{\tau_P} \left(\hat{c}_l \frac{3}{2} \left((I_{q(2)} + I_{q(3)}) I_{d(2)} + (I_{q(2)} + I_{q(3)}) I_{q(2)} \right) - P_1 \right) \\ \frac{1}{\tau_Q} \left(\hat{c}_l \frac{3}{2} \left((I_{d(2)} + I_{d(3)}) I_{q(2)} - (I_{q(2)} + I_{q(3)}) I_{d(2)} \right) - Q_1 \right) \\ \frac{1}{\tau_V} \left(\hat{c}_l \sqrt{(I_{q(2)} + I_{q(3)})^2 + (I_{d(2)} + I_{d(3)})^2} - V_1 \right) \end{bmatrix} \tag{5.36}$$

The non-linear state equations in (5.36) must be linearized into the form $p\delta\bar{\mathbf{x}} = \mathbf{L}\delta\mathbf{x}$ before the system eigenvalues can be evaluated. The matrix $\mathbf{L}$ for this particular system is determined using (5.37), where the functions f_i correspond to the i^{th} row on the right side of (5.36).

$$\mathbf{L} = \begin{bmatrix} \frac{\partial f_1}{\partial I_{q(2)}} & \frac{\partial f_1}{\partial I_{d(2)}} & \frac{\partial f_1}{\partial I_{q(3)}} & \frac{\partial f_1}{\partial I_{d(3)}} & \frac{\partial f_1}{\partial \theta_{v(1)}} & \frac{\partial f_1}{\partial z_{(1)}} & \frac{\partial f_1}{\partial P_{(1)}} & \frac{\partial f_1}{\partial Q_{(1)}} & \frac{\partial f_1}{\partial V_{(1)}} \\ \frac{\partial f_2}{\partial I_{q(2)}} & \frac{\partial f_2}{\partial I_{d(2)}} & \frac{\partial f_2}{\partial I_{q(3)}} & \frac{\partial f_2}{\partial I_{d(3)}} & \frac{\partial f_2}{\partial \theta_{v(1)}} & \frac{\partial f_2}{\partial z_{(1)}} & \frac{\partial f_2}{\partial P_{(1)}} & \frac{\partial f_2}{\partial Q_{(1)}} & \frac{\partial f_2}{\partial V_{(1)}} \\ \vdots & \vdots & \vdots & \vdots & \vdots & \vdots & \vdots & \vdots & \vdots \\ \frac{\partial f_9}{\partial I_{q(2)}} & \frac{\partial f_9}{\partial I_{d(2)}} & \frac{\partial f_9}{\partial I_{q(3)}} & \frac{\partial f_9}{\partial I_{d(3)}} & \frac{\partial f_9}{\partial \theta_{v(1)}} & \frac{\partial f_9}{\partial z_{(1)}} & \frac{\partial f_9}{\partial P_{(1)}} & \frac{\partial f_9}{\partial Q_{(1)}} & \frac{\partial f_9}{\partial V_{(1)}} \end{bmatrix} \Bigg|_{\bar{\mathbf{x}}=\bar{\mathbf{x}}_0} \tag{5.37}$$

5.2.3 Root-locus plots and small-signal dynamics

To determine small-signal system stability of the system in Figure 5.4, the the eigenvalues of (5.37) were evaluated. Stability was achieved when all 9 eigenvalues associated with $\mathbf{L}$ satisfied $\mathrm{Re}(\lambda_i) < 0$ for all i. To gain insight into the relationship between the inverter control gains and stability, the eigenvalues were determined as the gains M_p, M_Q, K_p, and K_i were each individually varied. As each of the control gains, M_p, M_Q, and K_i, was increased, a Hopf bifurcation was encountered and the system became unstable. Small-signal system stability was maintained for all values of proportional gain K_p. Table 5.1 summarizes the minimum gain threshold that produced unstable eigenvalues in the right half of the complex plane. The results are expressed in terms of the typically used base gains, $K_{i(0)} = 120 \times 10^3$, $M_{q(0)} = 0.05$, and $M_{p(0)} = 1.25\pi$.

Table 5.1: Gain setting at system instability

Parameter	Threshold gain when $\mathrm{Re}\lambda > 0$
M_p	$151M_{p(0)}$
M_q	$21.25M_{q(0)}$
K_i	$4.7K_{i(0)}$

The root-locus plot corresponding to the control parameter M_p is shown in Figure 5.5. For clarity, the root-locus plot contains only the eigenvalues corresponding to the $j\omega$ axis crossing. To produce the root-locus plot, M_p was varied from $0.1M_{p(0)}$ up to $151M_{p(0)}$. The eigenvalues shown moved into the right-hand plane when the gain was increased to $151M_{p(0)}$.

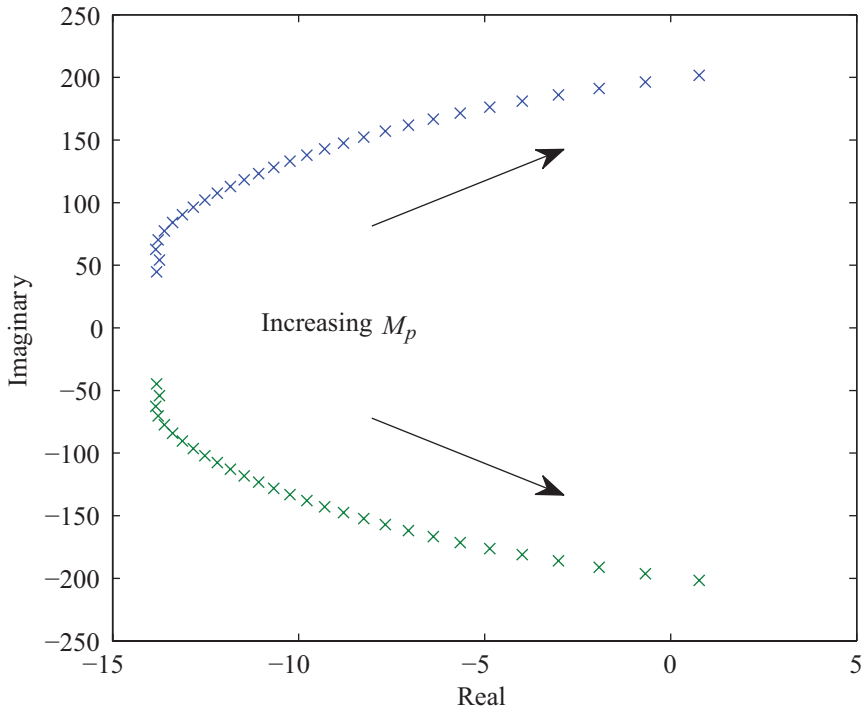

Figure 5.5: Root-locus plot with respect to the gain setting M_p

The dynamic responses of the inverter power output confirm the findings summarized in the root-locus plot of Figure 5.5. The exponentially growing output in Figure 5.6 corresponds to the minimum gain threshold setting that produced right-hand plane eigenvalues in Figure 5.5. This threshold gain setting for instability, $M_p = 151M_{p(0)}$, is summarized in Table 5.1. For a slightly smaller gain, $M_p = 141M_{p(0)}$, the eigenvalues are in the left-hand plane, and correspondingly, the response decays to a bounded output after a small disturbance.

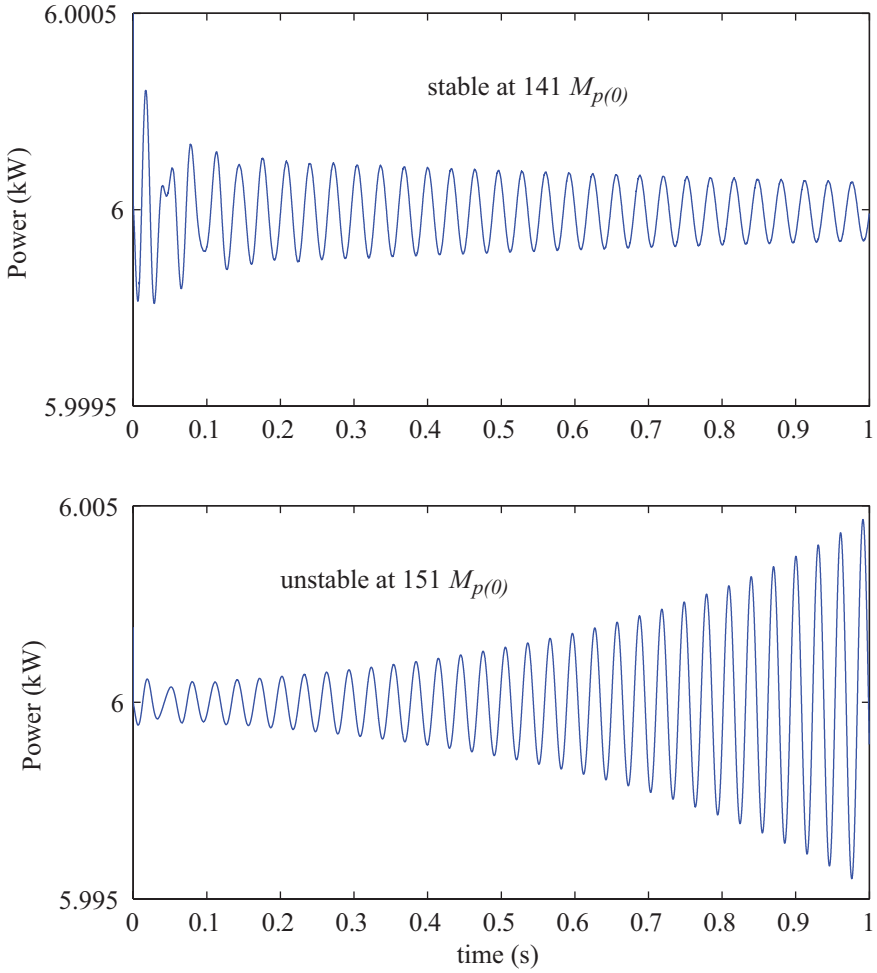

Figure 5.6: Stable and unstable dynamic responses of inverter power output

The root-locus plot corresponding to the control parameter M_q is shown in Figure 5.7. As before, the root-locus plot contains only the eigenvalues corresponding to the $j\omega$ axis crossing. The gain M_q was varied from $0.1M_{q(0)}$ up to $21.25M_{q(0)}$. The right-hand plane eigenvalues were produce for the gain setting $M_q = 21.25M_{q(0)}$.

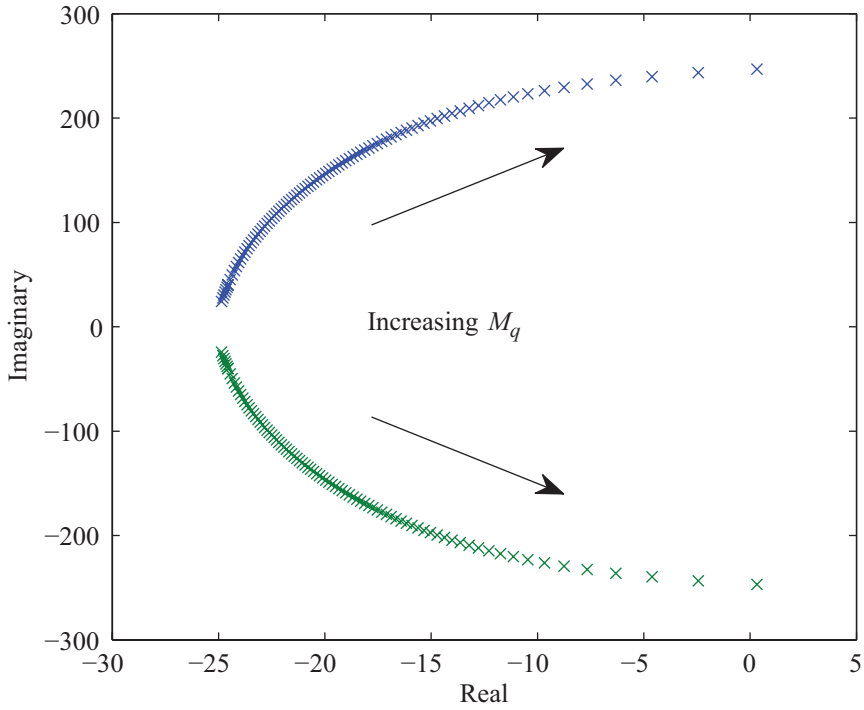

Figure 5.7: Root-locus plot with respect to the gain setting M_q

The dynamic responses of the inverter power output confirm the findings summarized in the root-locus plot of Figure 5.7. The exponentially growing output in Figure 5.8 corresponds the threshold gain setting for instability, $M_q = 21.25 M_{q(0)}$, as summarized in Table 5.1. For a slightly smaller gain, $M_q = 20.75 M_{q(0)}$, the eigenvalues are in the left-hand plane, and correspondingly, the response decays to a bounded output.

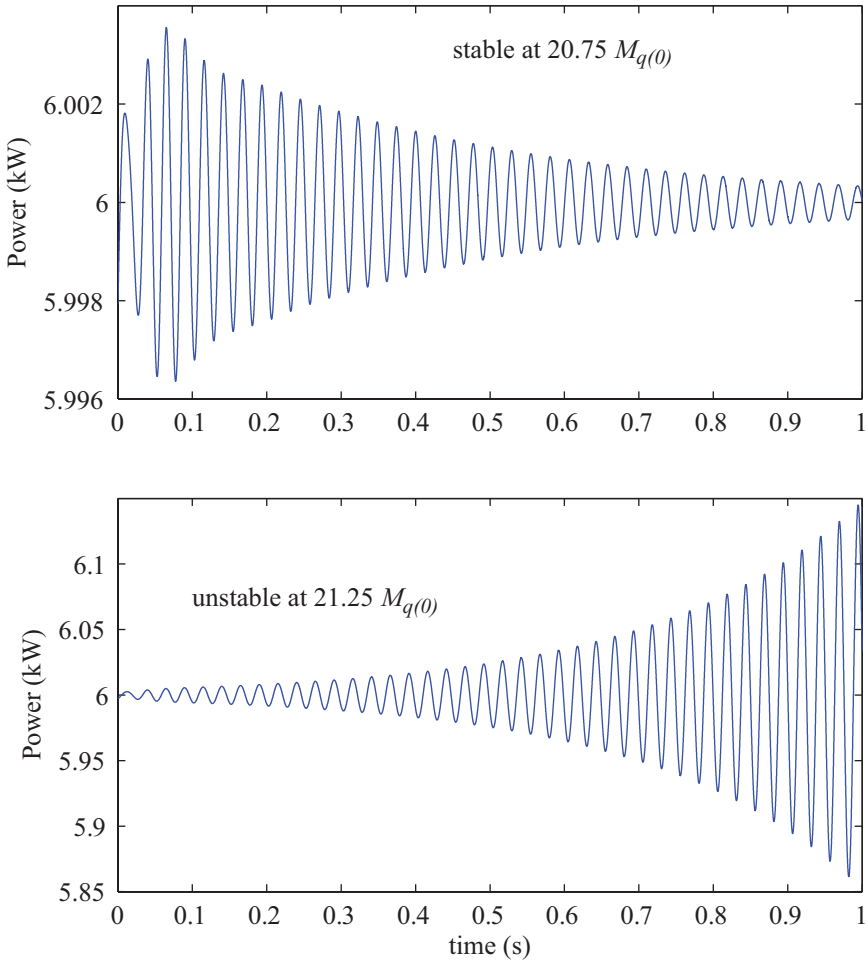

Figure 5.8: Stable and unstable dynamic responses of inverter power output

The root-locus plot corresponding to the control parameter K_i is shown in Figure 5.9. To produce the root-locus plot, K_i was varied from $0.1K_{i(0)}$ up to $4.7K_{i(0)}$. The eigenvalues shown moved into the right-hand plane when the gain was increased to $4.7K_{i(0)}$.

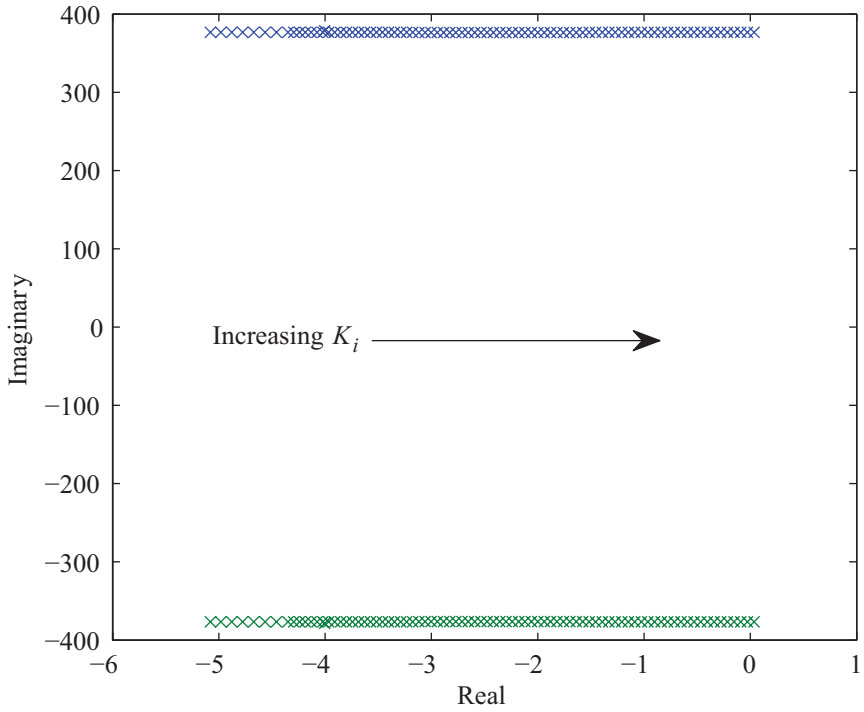

Figure 5.9: Root-locus plot with respect to the gain setting K_i

The dynamic responses of the inverter power output confirm the findings summarized in Figure 5.9. The exponentially growing output in Figure 5.10 corresponds to the minimum gain threshold setting that produced right-hand plane eigenvalues in Figure 5.9. This threshold gain setting for instability, $K_i = 4.7K_{i(0)}$, is as summarized in Table 5.1. For a slightly smaller gain, $K_i = 4.5K_{i(0)}$, the eigenvalues are in the left-hand plane, and correspondingly, the response decays to a bounded output after a small disturbance.

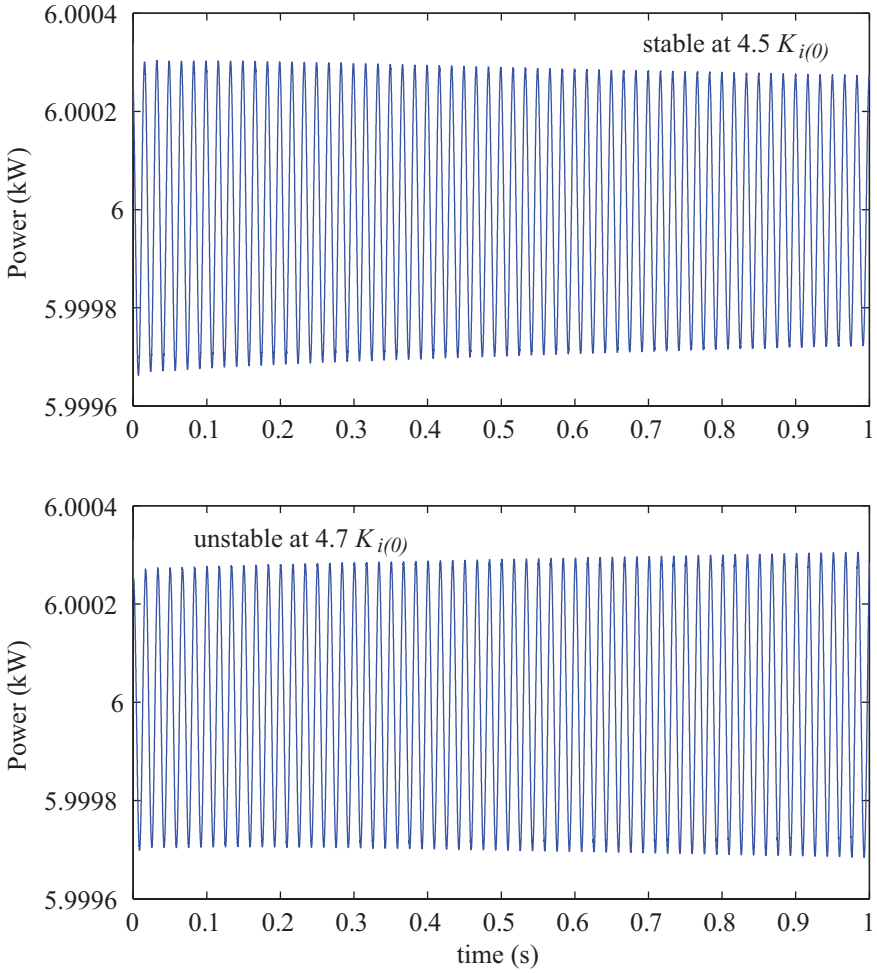

Figure 5.10: Stable and unstable dynamic responses of inverter power output

5.2.4 Summary

The ASMG and inverter state equations were transformed using Park's transformation, written in terms of states, and combined to form the non-linear system equations. After linearization, the eigenvalues of the example system were calculated and analyzed with respect to the inverter control gains. The root-locus plots summarized the relationship between the gain settings and the eigenvalue locations. The eigenvalue analysis was then confirmed by the stable and unstable dynamic responses of the inverter power output. As each of the control gains, M_p, M_Q, and K_i, was increased, a Hopf bifurcation was encountered and the system became unstable. Small-signal system stability was maintained for all values of proportional gain K_p. The relative change in gain required for instability was smallest for the parameter K_i. Therefore, it can be concluded that system stability was most sensitive to the gain K_i.

CHAPTER 6

CONCLUSION

Time domain simulations of microgrids have been conducted extensively using nodal based simulators such as EMTP. Although this type of software can provide detailed modeling of the system transient response, eigenvalues cannot be derived for the purpose of system stability and control analysis. For the purposes of stability analysis, state-variable models have been used. Because previously established state-variable models are based on linearized equations, the system response to large-transients is not valid. Furthermore, significant effort may be required to formulate the separate component models and system equations.

In this work, the ASMG algorithm was used to formulate a state-space model of the microgrid network, transformers, loads, grid-utility, and three-phase switch. Using ASMG, the microgrid was described by the branch parameters and circuit topology. The system state-equations were then derived systematically and there was no need to formulate the differential equations explicitly. The non-linear inverter models and controllers were implemented using Simulink. This non-linear model was then used to simulate the system response during the transition from grid-connected to islanded. The results provided a detailed system response and were verified using experimental measurements.

To conduct stability analysis of a sample system containing no transformers, the non-linear system equations were linearized and the system-level eigenvalues were analyzed with respect to the inverter control parameters. The relationship between the eigenvalues and control parameters was summarized in root-locus plots. The dynamic response of the system during stable and unstable conditions was consistent with the eigenvalue locations shown in the root-locus plots.

The presented methods can be used for computer-aided design of microgrid systems. A power system designer can simulate the dynamic

response of a proposed microgrid in addition to analyzing the system eigenvalues and stability. With the capability to quantitatively analyze a given design before implementation, decisions based on assumptions, estimations, and educated guesses can be minimized. Specifically, with the given insight, the analyst can make more informed choices for inverter control gains and system parameters.

6.1 Future Work

In Chapter 4, the presented formulation for the small-signal model required specific branch numberings in order for the *abc* to *qd*0 transformation to be valid. Furthermore, the microgrid system could not contain transformers. Future efforts will aim to create a generalized method for deriving small-signal models of any microgrid system containing transformers. Arbitrary branch numberings will also be possible. This will be achieved by performing the *abc* to *qd*0 transformation first before any model is formulated. The new *qd*0 circuit resulting from the transformation will be modeled using the ASMG algorithm and linearization will be performed directly on the transformed state equations. The resulting method will yield a method for evaluating the stability of any three-phase microgrid.

APPENDIX A

MICROGRID PARAMETERS

Table A.1 summarizes the microgrid system parameters.

Table A.1: These parameters correspond to the case studies examined in Chapter 5

$r_1 = 18.9$ mH	$L_1 = 49.4$ mH
$r_2 = 4.20$ mΩ	$L_2 = 59.1$ mH
$r_3 = 47.4$ mΩ	$L_3 = 66.5$ mH
$r_4 = 15.8$ mΩ	$L_4 = 22.2$ mH
$r_{\text{inv}} = 12.8$ mΩ	$L_{\text{inv}} = 5$ mH
$R_{\text{loadA}} = 9.6\ \Omega$	$R_{\text{loadB}} = 4.8\ \Omega$
$r_{\text{TA(480V)}} = 30.7$ mΩ	$L_{\text{TA(480V)}} = 407.4$ mH
$r_{\text{TA(208V)}} = 1.9$ mΩ	$L_{\text{TA(208V)}} = 25.5$ mH
$r_{\text{TB(480V)}} = 51.2$ mΩ	$L_{\text{TB(480V)}} = 679.1$ mH
$r_{\text{TB(208V)}} = 3.2$ mΩ	$L_{\text{TB(208V)}} = 42.4$ mH

APPENDIX B

LARGE-TRANSIENT SIMULATION CODE

This appendix contains the code and Simulink block diagrams (Figures B.1-B.4) used to model the dual-inverter microgrid.

```
%Microgrid with complete transformer models, two inverters,...
%and three loads
clear all
% base values
w0 = 2*pi*60;   %freq base
Sbase = 15e3; %single-phase power base
Vbase = 120; %line-neutral rms voltage
Vbase_high = 480/sqrt(3);
Ibase = Sbase/(3*Vbase);    %current base

%maximum power available from each generator in per unit
Pmax = 1.0;
Pmin = 0.0;

%filtering and limiter parameters for both generator models
Kp = 750*0.001;
Ki = 750*160;
Kplim = 3;
Kilim = 30;
tauf = 0.03;

%more parameters for generator model
mQ = 0.05;
mP = 1.25*pi;

%transmission line parameters
%impedances per mile
r_awg1 = 0.555;
x_awg1 = 0.546;
```

```
r_awg2 = 0.881;
x_awg2 = 0.574;
r_awg3 = 1.112;
x_awg3 = 0.588;

%total line resistance and inductance
Rline1 = (180/5280)*r_awg1;
Lline1 = (180/5280)*x_awg1/w0;
Rline2 = (20/5280)*r_awg3;
Lline2 = (20/5280)*x_awg3/w0;
Rline3 = (75*3/5280)*r_awg3;
Lline3 = (75*3/5280)*x_awg3/w0;
Rline4 = (25*3/5280)*r_awg3;
Lline4 = (25*3/5280)*x_awg3/w0;
Rline2_n = (20/5280)*r_awg2;
Lline2_n = (20/5280)*x_awg2/w0;
Rline3_n = (75*3/5280)*r_awg2;
Lline3_n = (75*3/5280)*x_awg2/w0;
Rline4_n = (25*3/5280)*r_awg2;
Lline4_n = (25*3/5280)*x_awg2/w0;

%transformer parameters
L_TG_high = (480^2*0.05/75000)*(1+1000)/w0;
R_TG_high = 480^2*0.01/75000;
L_TG_low = (120^2*0.05/75000)*(1+1000)/w0;
R_TG_low = 120^2*0.01/75000;
L_TM_high = (480^2*0.05/45000)*(1+1000)/w0;
R_TM_high = 480^2*0.01/45000;
L_TM_low = (120^2*0.05/45000)*(1+1000)/w0;
R_TM_low = 120^2*0.01/45000;
Rload1 = (120*sqrt(3))^2/(.3*Sbase); %R = VLL^2/Pload Y load
Rload2 = (120*sqrt(3))^2/(.3*Sbase);
Rload3 = (120*sqrt(3))^2/(.6*Sbase);
Lload = 0;

R10 = Rline1;   R38 = R10;  R39 = R10;
R1 = R_TG_high; R3 = R1;    R34 = R1;
R2 = R_TG_low+Rline2;   R4 = R2; R5 = R2;
R30 = 0;    R11 = 0;    R31 = 0;
R6 = R_TM_high; R8 = R6;    R29 = R6;
R7 = R_TM_low;  R27 = R7;   R28 = R7;
R33 = Rload1; R9 = R33; R32 = R33;
R12 = Rline3;   R22 = R12;  R23 = R12;
R37 = Rload2;    R13 = R37;    R36 = R37;
```

```
R14 = Rline4;   R24 = R14;  R25 = R14;
R15 = 0;    R41 = R15;  R42 = R15;
R17 = R_TM_high;    R19 = R17;  R40 = R17;
R18 = R_TM_low; R20 = R18;  R21 = R18;
R16 = Rload3; R44 = R16; R43 = R16;
R35 = Rline2_n;
R26 = Rline2_n+Rline3_n+Rline4_n;

rnet = [R1 R2 R3 R4 R5 R6 R7 R8 R9 R10...
R11 R12 R13 R14 R15 R16 R17 R18 R19 R20...
R21 R22 R23 R24 R25 R26 R27 R28 R29 R30...
R31 R32 R33 R34 R35 R36 R37 R38 R39 R40...
R41 R42 R43 R44];

%RESISTANCES
R_br0 = R_br0(rnet);

Linv = 1.88/w0;

L10 = Lline1;   L38 = L10;  L39 = L10;
L1 = L_TG_high; L3 = L1;    L34 = L1;
L2 = L_TG_low+Lline2;   L4 = L2; L5 = L2;
L30 = Linv; L11 = L30; L31 = L30;
L6 = L_TM_high; L8 = L6;    L29 = L6;
L7 = L_TM_low;  L27 = L7;   L28 = L7;
L33 = Lload;    L9 = Lload; L32 = Lload;
L12 = Lline3;   L22 = L12;  L23 = L12;
L37 = Lload;    L13 = Lload;    L36 = Lload;
L14 = Lline4;   L24 = L14;  L25 = L14;
L15 = Linv;    L41 = L15;  L42 = L15;
L17 = L_TM_high;    L19 = L17;  L40 = L17;
L18 = L_TM_low; L20 = L18;  L21 = L18;
L16 = Lload;    L44 = Lload;    L43 = Lload;
L35 = Lline2_n;
L26 = Lline2_n+Lline3_n+Lline4_n;

Lnet = [L1  L2  L3  L4  L5  L6  L7  L8 L9 L10...
L11 L12 L13 L14 L15 L16 L17 L18 L19 L20...
L21 L22 L23 L24 L25 L26 L27 L28 L29 L30...
L31 L32 L33 L34 L35 L36 L37 L38 L39 L40...
L41 L42 L43 L44];

%INDUCTANCES
L_br0 = L_br0(Lnet);
```

```
% e_br = [zeros(1,8) V12(4)' V12(1)' zeros(1,6) V12(5:6)'...
 0 V12(2:3)']';

%transformer mutual inductances
%grid interface transformer
M1 = 1000*sqrt((480^2*0.05/75000)*(120^2*0.05/75000)/(w0^2));
%microsource transformer
M2 = 1000*sqrt((480^2*0.05/45000)*(120^2*0.05/45000)/(w0^2));

%INCIDENCE MATRIX
Aa0.m

V1pk = Vbase_high*sqrt(2);

E1_req = 1;
P_req1 = 0.4;
P_req2 = 0.4;
q1_disc = 15/60;    %disconnection time

[nmax,bmax] = size(Aa0);   %maximum number of branches and nodes
imax = 21; %maximum number state-variable currents

%initial values of state variables
% i_initial = zeros(imax,1);%#ok<NASGU>
% int1_PI_initial = 0;%#ok<NASGU>
% int1_theta_initial = 0;%#ok<NASGU>
% int1_P_initial = 0;%#ok<NASGU>
% int1_Q_initial = 0;%#ok<NASGU>
% int1_Pmin_initial = 0;%#ok<NASGU>
% int1_Pmax_initial = 0;%#ok<NASGU>
% int1_Vrms_initial = 0;%#ok<NASGU>
% int2_PI_initial = 0;%#ok<NASGU>
% int2_theta_initial = 0;%#ok<NASGU>
% int2_P_initial = 0;%#ok<NASGU>
% int2_Q_initial = 0;%#ok<NASGU>
% int2_Pmin_initial = 0;%#ok<NASGU>
% int2_Pmax_initial = 0;%#ok<NASGU>
% int2_Vrms_initial = 0;%#ok<NASGU>
% theta_V1_initial = 0;%#ok<NASGU>

load y1_old_8_29_9pt24.mat;

theta_V1_initial = xFinal111(1); %#ok<NASGU>
```

```
int1_Q_initial = xFinal111(2); %#ok<NASGU>
int1_Vrms_initial = xFinal111(3); %#ok<NASGU>
int1_PI_initial = xFinal111(4); %#ok<NASGU>
int1_theta_initial = xFinal111(5); %#ok<NASGU>
int2_Q_initial = xFinal111(6); %#ok<NASGU>
int2_Vrms_initial = xFinal111(7); %#ok<NASGU>
int2_PI_initial = xFinal111(8); %#ok<NASGU>
int2_theta_initial = xFinal111(9); %#ok<NASGU>
i_initial = xFinal111(10:30);%#ok<NASGU>
int1_P_initial = xFinal111(31); %#ok<NASGU>
int1_Pmax_initial = xFinal111(32); %#ok<NASGU>
int1_Pmin_initial = xFinal111(33); %#ok<NASGU>
int2_P_initial = xFinal111(34); %#ok<NASGU>
int2_Pmax_initial = xFinal111(35); %#ok<NASGU>
int2_Pmin_initial = xFinal111(36); %#ok<NASGU>
int_P_flows = [5.842714268748392e+003;...
 2.848369209528618e+003];%#ok<NASGU>
int1_Irms_initial = 16.708993634864019;%#ok<NASGU>
int2_Irms_initial = 18.243670782633664;%#ok<NASGU>

Aa = Aa0;
L_br = L_br0;%#ok<NASGU>
R_br = R_br0;%#ok<NASGU>
[A_ss,B_ss,C_ss,D_ss] = Bb_trans(Aa,R_br,L_br);%#ok<NASGU>
%
% t_total_loop = 20;
% Nmax = t_total_loop/q1_disc;
% n=1;
%
% while n <= Nmax
% theta_V1_initial = xFinal111(1); %#ok<NASGU>
% int1_Q_initial = xFinal111(2); %#ok<NASGU>
% int1_Vrms_initial = xFinal111(3); %#ok<NASGU>
% int1_PI_initial = xFinal111(4); %#ok<NASGU>
% int1_theta_initial = xFinal111(5); %#ok<NASGU>
% int2_Q_initial = xFinal111(6); %#ok<NASGU>
% int2_Vrms_initial = xFinal111(7); %#ok<NASGU>
% int2_PI_initial = xFinal111(8); %#ok<NASGU>
% int2_theta_initial = xFinal111(9); %#ok<NASGU>
% i_initial = xFinal111(10:30);%#ok<NASGU>
% int1_P_initial = xFinal111(31); %#ok<NASGU>
% int1_Pmax_initial = xFinal111(32); %#ok<NASGU>
% int1_Pmin_initial = xFinal111(33); %#ok<NASGU>
% int2_P_initial = xFinal111(34); %#ok<NASGU>
```

```
% int2_Pmax_initial = xFinal111(35); %#ok<NASGU>
% int2_Pmin_initial = xFinal111(36); %#ok<NASGU>
% clear xFinal111;

[t1,x1,y1] = sim('two_inv_complete_111');
%
% clear t1;
% clear x1;
% clear y1;
%
% n = n+1;
% end

%variables before 1st phase disconnection
V1rms_1 = y1(:,1);
I1rms_1 = y1(:,2);
freq1_1 = y1(:,3);
P1_1 = y1(:,4);
Q1_1 = y1(:,5);
V2rms_1 = y1(:,6);
I2rms_1 = y1(:,7);
freq2_1 = y1(:,8);
P2_1 = y1(:,9);
Q2_1 = y1(:,10);
Flow1_1 = y1(:,11);
Flow2_1 = y1(:,12);
P1_unf_1 = y1(:,13);
Q1_unf_1 = y1(:,14);
V1_unf_1 = y1(:,15);
I1_unf_1 = y1(:,16);
P2_unf_1 = y1(:,17);
Q2_unf_1 = y1(:,18);
V2_unf_1 = y1(:,19);
I2_unf_1 = y1(:,20);
F1_unf_1 = y1(:,21);
F2_unf_1 = y1(:,22);

%initial values for simulation #2
t2_initial = t1(length(t1));
int1_Vrms_initial = xFinal111(1); %#ok<NASGU>
int1_Irms_initial = xFinal111(2); %#ok<NASGU>
int1_P_initial = xFinal111(3); %#ok<NASGU>
int1_Pmin_initial = xFinal111(4); %#ok<NASGU>
int1_Pmax_initial = xFinal111(5); %#ok<NASGU>
```

```
int1_Q_initial = xFinal111(6); %#ok<NASGU>
int2_Vrms_initial = xFinal111(7); %#ok<NASGU>
int2_Irms_initial = xFinal111(8); %#ok<NASGU>
int2_P_initial = xFinal111(9); %#ok<NASGU>
int2_Pmin_initial = xFinal111(10); %#ok<NASGU>
int2_Pmax_initial = xFinal111(11); %#ok<NASGU>
int2_Q_initial = xFinal111(12); %#ok<NASGU>
int_P_flows = xFinal111(13:14); %#ok<NASGU>
theta_V1_initial = xFinal111(15); %#ok<NASGU>
int1_PI_initial = xFinal111(16); %#ok<NASGU>
int1_theta_initial = xFinal111(17); %#ok<NASGU>
int2_PI_initial = xFinal111(18); %#ok<NASGU>
int2_theta_initial = xFinal111(19); %#ok<NASGU>
i_initial = xFinal111(21:40);%#ok<NASGU>


%system matrices
Aa(:,2) = []; %#ok<NASGU>
L_br(:,2) = [];%#ok<NASGU>
L_br(2,:) = [];%#ok<NASGU>
R_br(:,2) = [];%#ok<NASGU>
R_br(2,:) = [];%#ok<NASGU>
clear Bb_trans
[A_ss,B_ss,C_ss,D_ss] = Bb_trans(Aa,R_br,L_br);%#ok<NASGU>
[t2,x2,y2] = sim('two_inv_complete_011');

%variables before 2nd phase disconnection
V1rms_2 = y2(:,1);
I1rms_2 = y2(:,2);
freq1_2 = y2(:,3);
P1_2 = y2(:,4);
Q1_2 = y2(:,5);
V2rms_2 = y2(:,6);
I2rms_2 = y2(:,7);
freq2_2 = y2(:,8);
P2_2 = y2(:,9);
Q2_2 = y2(:,10);
Flow1_2 = y2(:,11);
Flow2_2 = y2(:,12);
P1_unf_2 = y2(:,13);
Q1_unf_2 = y2(:,14);
V1_unf_2 = y2(:,15);
I1_unf_2 = y2(:,16);
P2_unf_2 = y2(:,17);
```

```
Q2_unf_2 = y2(:,18);
V2_unf_2 = y2(:,19);
I2_unf_2 = y2(:,20);
F1_unf_2 = y2(:,21);
F2_unf_2 = y2(:,22);

%initial values for simulation #3
t3_initial = t2_initial + t2(length(t2));
int1_Vrms_initial = xFinal011(1); %#ok<NASGU>
int1_Irms_initial = xFinal011(2); %#ok<NASGU>
int1_P_initial = xFinal011(3); %#ok<NASGU>
int1_Pmin_initial = xFinal011(4); %#ok<NASGU>
int1_Pmax_initial = xFinal011(5); %#ok<NASGU>
int1_Q_initial = xFinal011(6); %#ok<NASGU>
int2_Vrms_initial = xFinal011(7); %#ok<NASGU>
int2_Irms_initial = xFinal011(8); %#ok<NASGU>
int2_P_initial = xFinal011(9); %#ok<NASGU>
int2_Pmin_initial = xFinal011(10); %#ok<NASGU>
int2_Pmax_initial = xFinal011(11); %#ok<NASGU>
int2_Q_initial = xFinal011(12); %#ok<NASGU>
int_P_flows = xFinal011(13:14); %#ok<NASGU>
theta_V1_initial = xFinal011(15); %#ok<NASGU>
int1_PI_initial = xFinal011(16); %#ok<NASGU>
int1_theta_initial = xFinal011(17); %#ok<NASGU>
int2_PI_initial = xFinal011(18); %#ok<NASGU>
int2_theta_initial = xFinal011(19); %#ok<NASGU>
i_initial = xFinal011(21:39);%#ok<NASGU>

%system matrices
Aa(:,4) = []; %#ok<NASGU>
L_br(:,4) = [];%#ok<NASGU>
L_br(4,:) = [];%#ok<NASGU>
R_br(:,4) = [];%#ok<NASGU>
R_br(4,:) = [];%#ok<NASGU>
clear Bb_trans
[A_ss,B_ss,C_ss,D_ss] = Bb_trans(Aa,R_br,L_br);%#ok<NASGU>
[t3,x3,y3] = sim('two_inv_complete_010');

%variables before 3rd phase disconnection
V1rms_3 = y3(:,1);
I1rms_3 = y3(:,2);
freq1_3 = y3(:,3);
P1_3 = y3(:,4);
Q1_3 = y3(:,5);
```

```
V2rms_3 = y3(:,6);
I2rms_3 = y3(:,7);
freq2_3 = y3(:,8);
P2_3 = y3(:,9);
Q2_3 = y3(:,10);
Flow1_3 = y3(:,11);
Flow2_3 = y3(:,12);
P1_unf_3 = y3(:,13);
Q1_unf_3 = y3(:,14);
V1_unf_3 = y3(:,15);
I1_unf_3 = y3(:,16);
P2_unf_3 = y3(:,17);
Q2_unf_3 = y3(:,18);
V2_unf_3 = y3(:,19);
I2_unf_3 = y3(:,20);
F1_unf_3 = y3(:,21);
F2_unf_3 = y3(:,22);

%initial values for simulation #4
t4_initial = t3_initial + t3(length(t3));
int1_Vrms_initial = xFinal010(1); %#ok<NASGU>
int1_Irms_initial = xFinal010(2); %#ok<NASGU>
int1_P_initial = xFinal010(3); %#ok<NASGU>
int1_Pmin_initial = xFinal010(4); %#ok<NASGU>
int1_Pmax_initial = xFinal010(5); %#ok<NASGU>
int1_Q_initial = xFinal010(6); %#ok<NASGU>
int2_Vrms_initial = xFinal010(7); %#ok<NASGU>
int2_Irms_initial = xFinal010(8); %#ok<NASGU>
int2_P_initial = xFinal010(9); %#ok<NASGU>
int2_Pmin_initial = xFinal010(10); %#ok<NASGU>
int2_Pmax_initial = xFinal010(11); %#ok<NASGU>
int2_Q_initial = xFinal010(12); %#ok<NASGU>
int_P_flows = xFinal010(13:14); %#ok<NASGU>
theta_V1_initial = xFinal010(15); %#ok<NASGU>
int1_PI_initial = xFinal010(16); %#ok<NASGU>
int1_theta_initial = xFinal010(17); %#ok<NASGU>
int2_PI_initial = xFinal010(18); %#ok<NASGU>
int2_theta_initial = xFinal010(19); %#ok<NASGU>
i_initial = xFinal010(21:38);%#ok<NASGU>

%system matrices
Aa(:,3) = [];
L_br(:,3) = [];%#ok<NASGU>
L_br(3,:) = [];
```

```
R_br(:,3) = [];%#ok<NASGU>
R_br(3,:) = [];
clear Bb_trans
[A_ss,B_ss,C_ss,D_ss] = Bb_trans(Aa,R_br,L_br);%#ok<NASGU>
tstop = 15/60;
[t4,x4,y4] = sim('two_inv_complete_000',tstop);

%variables after islanding
V1rms_4 = y4(:,1);
I1rms_4 = y4(:,2);
freq1_4 = y4(:,3);
P1_4 = y4(:,4);
Q1_4 = y4(:,5);
V2rms_4 = y4(:,6);
I2rms_4 = y4(:,7);
freq2_4 = y4(:,8);
P2_4 = y4(:,9);
Q2_4 = y4(:,10);
Flow1_4 = y4(:,11);
Flow2_4 = y4(:,12);
P1_unf_4 = y4(:,13);
Q1_unf_4 = y4(:,14);
V1_unf_4 = y4(:,15);
I1_unf_4 = y4(:,16);
P2_unf_4 = y4(:,17);
Q2_unf_4 = y4(:,18);
V2_unf_4 = y4(:,19);
I2_unf_4 = y4(:,20);
F1_unf_4 = y4(:,21);
F2_unf_4 = y4(:,22);

%concatenation of results to create unified waveforms
V1rms = [V1rms_1; V1rms_2; V1rms_3; V1rms_4];
I1rms = [I1rms_1; I1rms_2; I1rms_3; I1rms_4];
freq1 = [freq1_1; freq1_2; freq1_3; freq1_4];
P1 = [P1_1; P1_2; P1_3; P1_4];
Q1 = [Q1_1; Q1_2; Q1_3; Q1_4];
V2rms = [V2rms_1; V2rms_2; V2rms_3; V2rms_4];
I2rms = [I2rms_1; I2rms_2; I2rms_3; I2rms_4];
freq2 = [freq2_1; freq2_2; freq2_3; freq2_4];
P2 = [P2_1; P2_2; P2_3; P2_4];
Q2 = [Q2_1; Q2_2; Q2_3; Q2_4];
Flow1 = [Flow1_1; Flow1_2; Flow1_3; Flow1_4];
Flow2 = [Flow2_1; Flow2_2; Flow2_3; Flow2_4];
```

```
P1_unf = [P1_unf_1; P1_unf_2; P1_unf_3; P1_unf_4];
Q1_unf = [Q1_unf_1; Q1_unf_2; Q1_unf_3; Q1_unf_4];
V1_unf = [V1_unf_1; V1_unf_2; V1_unf_3; V1_unf_4];
I1_unf = [I1_unf_1; I1_unf_2; I1_unf_3; I1_unf_4];
P2_unf = [P2_unf_1; P2_unf_2; P2_unf_3; P2_unf_4];
Q2_unf = [Q2_unf_1; Q2_unf_2; Q2_unf_3; Q2_unf_4];
V2_unf = [V2_unf_1; V2_unf_2; V2_unf_3; V2_unf_4];
I2_unf = [I2_unf_1; I2_unf_2; I2_unf_3; I2_unf_4];
F1_unf = [F1_unf_1; F1_unf_2; F1_unf_3; F1_unf_4];
F2_unf = [F2_unf_1; F2_unf_2; F2_unf_3; F2_unf_4];

t = [t1; t2+t2_initial; t3+t3_initial; t4+t4_initial];
tend = t(length(t));
```

This function calculates the ASMG state-space model matrix coefficients.

```
function [A_ss,B_ss,C_ss,D_ss] = Bb_trans(Aa,R_br,L_br)

[n,b] = size(Aa);
Aa_rref = rref(Aa);
A_hat = Aa_rref(1:(n-1),n:b);  %produces reduced row-eschelon form
Bb_t = [-A_hat; eye(b-n+1)];

[b,w] = size(Bb_t); %#ok<NASGU>
Bb = Bb_t';
Rx = Bb*R_br*Bb_t;
Lx = Bb*L_br*Bb_t;
A_ss = -inv(Lx)*Rx;
B_ss = -inv(Lx)*Bb;
C_ss = [Bb_t;R_br*Bb_t-L_br*Bb_t*inv(Lx)*Rx];
D_ss = [zeros(b);eye(b)-L_br*Bb_t*inv(Lx)*Bb];

return
```

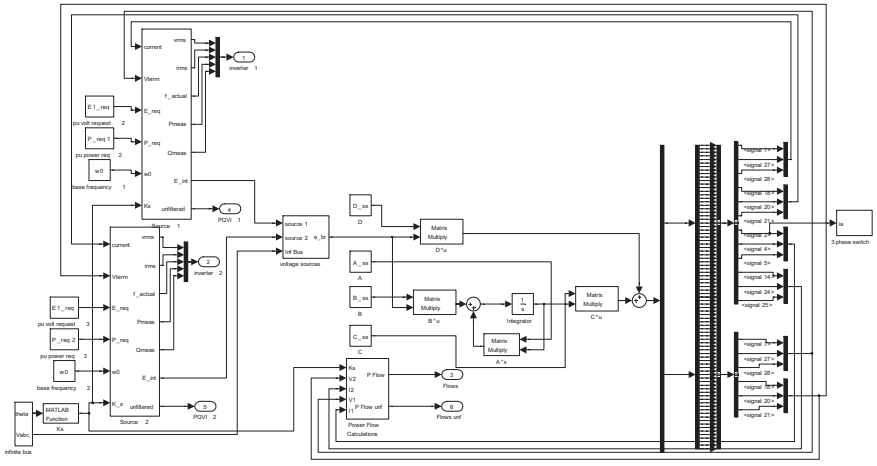

Figure B.1: Simulink block diagram of the microgrid model

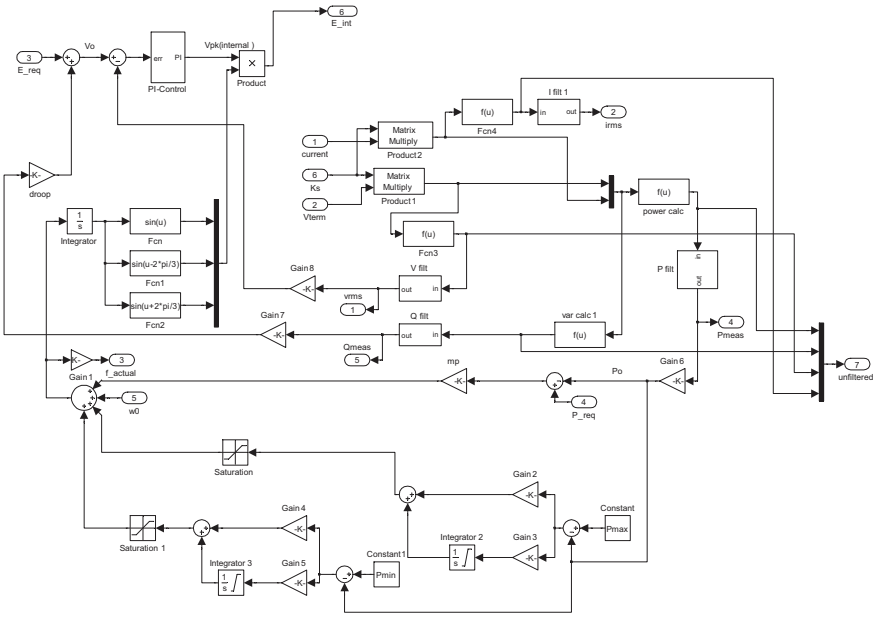

Figure B.2: Block diagram of the inverter model

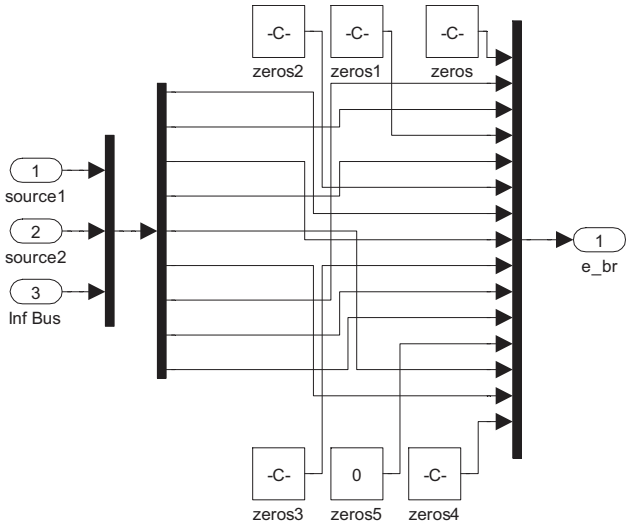

Figure B.3: Signal routing block to create voltage source vector $\mathbf{e}_{br}$

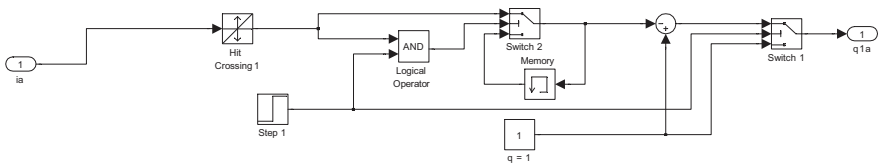

Figure B.4: Current zero-crossing detector for three-phase switch

APPENDIX C

SMALL-SIGNAL ANALYSIS CODE

This appendix contains the code and Simulink block diagram (Figure C.1) used to model and analyze the single-inverter microgrid.

This function below calculates the equilibrium values and eigenvalues of the model as the gain M_p is varied. Similar code is used to evaluate the eigenvalues with respect to M_q, K_1, and K_p

```
%modal analysis for microgrid with one inverter, one load, and
%no tranformers while grid connected
close all
clear all

% base values
w0 = 2*pi*60;   %freq base
Sbase = 15e3; %single-phase power base
Vbase = 120; %line-neutral rms voltage

%filtering and limiter parameters for inverter
Kp = 750*0.001;
Ki = 750*160;
tau_P = 0.03;

% base values
w0 = 2*pi*60;   %freq base
Sbase = 15e3; %single-phase power base
Vbase = 120; %line-neutral rms voltage
Ibase = Sbase/(3*Vbase);

%maximum power available from each generator in per unit
Pmax = 1.0;
Pmin = 0.0;

%filtering and limiter parameters for inverter
Kp = 750*0.001;
```

```
Ki = 750*160;
Kplim = 3;
Kilim = 30;
tauf = 0.03;

%more parameters for inverter model
mQ = 0.05;
mP = 1.25*pi;

%transmission line parameters
%impedances per mile
r_awg1 = 0.555;
x_awg1 = 0.546;
r_awg3 = 1.112;
x_awg3 = 0.588;

%total line resistance and inductance
Rline1 = (180/5280)*r_awg1;
Lline1 = (180/5280)*x_awg1/w0;
Rline2 = (20/5280)*r_awg3;
Lline2 = (20/5280)*x_awg3/w0;

%CIRCUIT PARAMETERS
N = (208/480);  %turns ratio

%transformer parameters
L_TG_high = (480^2*0.05/75000)/w0;
R_TG_high = 480^2*0.01/75000;
L_TG_low = (120^2*0.05/75000)/w0;
R_TG_low = 120^2*0.01/75000;
L_TM_high = (480^2*0.05/45000)/w0;
R_TM_high = 480^2*0.01/45000;
L_TM_low = (120^2*0.05/45000)/w0;
R_TM_low = 120^2*0.01/45000;
Rload = (120*sqrt(3))^2/9000; %R = VLL^2/Pload wye-connected load
Lload = 0;

R1_net = Rload;
R2_net = R_TM_high*N^2+R_TM_low;
R3_net = (Rline1+R_TG_high)*N^2+Rline2+R_TG_low;

R1a = R1_net;  R1b = R1a;      R1c = R1a;
R2a = R2_net; R2b = R2a;      R2c = R2a;
R3a = R3_net;   R3b = R3a;      R3c = R3a;
```

```
R_br = [R1a 0 0   0   0   0   0   0   0;
        0   R1b 0   0   0   0   0   0   0;
        0   0   R1c 0   0   0   0   0   0;
        0   0   0   R2a 0   0   0   0   0;
        0   0   0   0   R2b 0   0   0   0;
        0   0   0   0   0   R2c 0   0   0;
        0   0   0   0   0   0   R3a 0   0;
        0   0   0   0   0   0   0   R3b 0;
        0   0   0   0   0   0   0   0   R3c];

L1_net = Lload;
L2_net = 1.88/w0+L_TM_high*N^2+L_TM_low;
L3_net = (Lline1+L_TG_high)*N^2+Lline2+L_TG_low;

L1a = L1_net;   L1b = L1a;      L1c = L1a;
L2a = L2_net;   L2b = L2a;      L2c = L2a;
L3a = L3_net;   L3b = L3a;      L3c = L3a;

L_br = [L1a 0 0   0   0   0   0   0   0;
        0   L1b 0   0   0   0   0   0   0;
        0   0   L1c 0   0   0   0   0   0;
        0   0   0   L2a 0   0   0   0   0;
        0   0   0   0   L2b 0   0   0   0;
        0   0   0   0   0   L2c 0   0   0;
        0   0   0   0   0   0   L3a 0   0;
        0   0   0   0   0   0   0   L3b 0;
        0   0   0   0   0   0   0   0   L3c];

%initial circuit configuration
Aa = [  1   0   0   1   0   0   1   0   0;
        0   1   0   0   1   0   0   1   0;
        0   0   1   0   0   1   0   0   1;
        -1  -1  -1  -1  -1  -1  -1  -1  -1];

V1pk = Vbase*sqrt(2);   %infinite bus voltage magnitude

E1_req = 1;     %voltage command
P_req = 0.4;    %power command
q1_disc = 10;

Aa0 = Aa;   L_br0 = L_br;   R_br0 = R_br;
[A_ss,B_ss,C_ss,D_ss] = Bb_trans(Aa,R_br,L_br);
```

```
w = w0;
a11 = A_ss(1,1);
a12 = A_ss(1,4);
a21 = A_ss(4,1);
a22 = A_ss(4,4);
b12 = B_ss(1,4);
b22 = B_ss(4,7);
cl = C_ss(10,1);

Tp = tauf;
Tq = Tp;
Tv = 0.001;

%steady state variables
load y1_old_9_4_9_pt2.mat;

ind_increase = (1:5:160);
ind_decrease = 1-(0:.1:.9);
Mp = mP*ind_decrease;

Rmax = 1.01;
Rmin = 1;
R_increase = (Rmin:(Rmax-Rmin)/length(ind_increase):Rmax);
R_decrease = (Rmin:(Rmax-Rmin)/length(ind_decrease):Rmax);
Rload = Rload*ind_decrease;

%preallocation of eigenvalue entries
Nmax = length(ind_increase)-1;
Mmax = length(ind_decrease)-1;
E1 = zeros(Nmax+Mmax-1,1);
E2 = zeros(Nmax+Mmax-1,1);
E3 = zeros(Nmax+Mmax-1,1);
E4 = zeros(Nmax+Mmax-1,1);
E5 = zeros(Nmax+Mmax-1,1);
E6 = zeros(Nmax+Mmax-1,1);
E7 = zeros(Nmax+Mmax-1,1);
E8 = zeros(Nmax+Mmax-1,1);
E9 = zeros(Nmax+Mmax-1,1);

m = 1; %initialize counter
while m<=Mmax-1;

initial_values_1 = [...
    y1_old(1:9) y1_old(27:34)];
```

```
i_2a0_1 = initial_values_1(4);
i_2b0_1 = initial_values_1(5);
i_2c0_1 = initial_values_1(6);
i_3a0_1 = initial_values_1(7);
i_3b0_1 = initial_values_1(8);
i_3c0_1 = initial_values_1(9);
i0_sim1 = [i_2a0_1,i_2b0_1,i_2c0_1,i_3a0_1,i_3b0_1,i_3c0_1]';
int1_PI_initial = initial_values_1(10);
int1_theta_initial = initial_values_1(11);
int1_P_initial = initial_values_1(12);
int1_Q_initial = initial_values_1(13);
int1_Pmin_initial = initial_values_1(14);
int1_Pmax_initial = initial_values_1(15);
int1_Vrms_initial = initial_values_1(16);
theta_V1_initial = initial_values_1(17);
z_eq = int1_PI_initial;
P_eq = int1_P_initial;
Q_eq = int1_Q_initial;
V_eq = int1_Vrms_initial;
theta_initial = theta_V1_initial;
delta_eq = int1_theta_initial-theta_initial;

%transformation to qd0 for currents
q= theta_initial;
Ks = (2/3)*[cos(q) cos(q-2*pi/3) cos(q+2*pi/3);
   sin(q) sin(q-2*pi/3) sin(q+2*pi/3);
   0.5 0.5 0.5];

i2qd0 = Ks*[i_2a0_1 i_2b0_1 i_2c0_1]';
i2q_eq = i2qd0(1);
i2d_eq = i2qd0(2);
i20_eq = i2qd0(3);

i3qd0 = Ks*[i_3a0_1 i_3b0_1 i_3c0_1]';
i3q_eq = i3qd0(1);
i3d_eq = i3qd0(2);
i30_eq = i3qd0(3);

Punf = -cl*(3/2)*((i2q_eq+i3q_eq)*i2q_eq+(i2d_eq+i3d_eq)*i2d_eq);
Qunf = -cl*(3/2)*(i3d_eq*i2q_eq-i3q_eq*i2d_eq);
Vunf = (-cl/sqrt(2))*sqrt((i2q_eq+i3q_eq)^2+(i2d_eq+i3d_eq)^2);

n1 = (3/2)*cl/Tp;
n2 = (3/2)*cl/Tq;
```

```
n3 = cl/(sqrt(2)*sqrt((i2d_eq+i3d_eq)^2+(i2q_eq+i3q_eq)^2)*Tv);

%linearized matrix
M = [a11 -w a12 0 -b12*(Kp*(E1_req+mQ*Q_eq/Sbase-V_eq/Vbase)+...
z_eq)*sin(delta_eq) b12*cos(delta_eq) 0 b12*Kp*mQ*...
cos(delta_eq)/Sbase -b12*Kp*cos(delta_eq)/Vbase;
    w a11 0 a12 -b12*(Kp*(E1_req +mQ*Q_eq/Sbase-V_eq/Vbase)+...
    z_eq)*cos(delta_eq) -b12*sin(delta_eq) 0 -b12*Kp*mQ*...
    sin(delta_eq)/Sbase b12*Kp*sin(delta_eq)/Vbase;
    a21 0 a22 -w 0 0 0 0 0;
    0 a21 w a22 0 0 0 0 0;
    0 0 0 0 0 0 -Mp(m)/Sbase 0 0;
    0 0 0 0 0 0 0 Ki*mQ/Sbase -Ki/Vbase;
    -n1*(2*i2q_eq+i3q_eq) -n1*(2*i2d_eq+i3d_eq) -n1*i2q_eq...
     -n1*i2d_eq 0 0 -1/Tp 0 0;
    -n2*i3d_eq n2*i3q_eq n2*i2d_eq -n2*i2q_eq 0 0 0 -1/Tq 0;
    -n3*(i2q_eq+i3q_eq) -n3*(i2d_eq+i3d_eq) -n3*(i2q_eq+...
    i3q_eq) -n3*(i2d_eq+i3d_eq) 0 0 0 0 -1/Tv];

Eig = eig(M);
E1(m+Nmax) = Eig(1);
E2(m+Nmax) = Eig(2);
E3(m+Nmax) = Eig(3);
E4(m+Nmax) = Eig(4);
E5(m+Nmax) = Eig(5);
E6(m+Nmax) = Eig(6);
E7(m+Nmax) = Eig(7);
E8(m+Nmax) = Eig(8);
E9(m+Nmax) = Eig(9);

mP = Mp(m+1);

R1_net = Rload(m+1);%#ok<NASGU>
R2_net = R_TM_high*N^2+R_TM_low;
R3_net = (Rline1+R_TG_high)*N^2+Rline2+R_TG_low;

R1a = R1_net;  R1b = R1a;      R1c = R1a;
R2a = R2_net; R2b = R2a;      R2c = R2a;
R3a = R3_net;   R3b = R3a;      R3c = R3a;

R_br = [R1a 0 0   0   0   0   0   0   0;
        0   R1b 0   0   0   0   0   0   0;
        0   0   R1c 0   0   0   0   0   0;
        0   0   0   R2a 0   0   0   0   0;
```

```
        0   0   0   0   R2b 0   0   0   0;
        0   0   0   0   0   R2c 0   0   0;
        0   0   0   0   0   0   R3a 0   0;
        0   0   0   0   0   0   0   R3b 0;
        0   0   0   0   0   0   0   0   R3c];

clear Bb_trans
[A_ss,B_ss,C_ss,D_ss] = Bb_trans(Aa,R_br,L_br);%#ok<NASGU>
a11 = A_ss(1,1);
a12 = A_ss(1,4);
a21 = A_ss(4,1);
a22 = A_ss(4,4);
b12 = B_ss(1,4);
b22 = B_ss(4,7);
cl = C_ss(10,1);

tstop = 5/60;
[t1,x1,y1] = sim('basic_test_sim_111',tstop);

y1_old = y1(length(y1),:);

m = m+1;
end

clear Mp;
clear mP;
clear Rload;
clear y1_old;

%steady state variables
load y1_old_9_4_9_pt2.mat;

mP = 1.25*pi;
Mp = mP*ind_increase;
Rload = (120*sqrt(3))^2/9000;
Rload = Rload*R_increase;

n = 1; %initialize counter
while n<=Nmax;

initial_values_1 = [...
    y1_old(1:9) y1_old(27:34)];
i_2a0_1 = initial_values_1(4);
i_2b0_1 = initial_values_1(5);
```

```
i_2c0_1 = initial_values_1(6);
i_3a0_1 = initial_values_1(7);
i_3b0_1 = initial_values_1(8);
i_3c0_1 = initial_values_1(9);
i0_sim1 = [i_2a0_1,i_2b0_1,i_2c0_1,i_3a0_1,i_3b0_1,i_3c0_1]';
int1_PI_initial = initial_values_1(10);
int1_theta_initial = initial_values_1(11);
int1_P_initial = initial_values_1(12);
int1_Q_initial = initial_values_1(13);
int1_Pmin_initial = initial_values_1(14);
int1_Pmax_initial = initial_values_1(15);
int1_Vrms_initial = initial_values_1(16);
theta_V1_initial = initial_values_1(17);
z_eq = int1_PI_initial;
P_eq = int1_P_initial;
Q_eq = int1_Q_initial;
V_eq = int1_Vrms_initial;
theta_initial = theta_V1_initial;
delta_eq = int1_theta_initial-theta_initial;

%transformation to qd0 for currents
q= theta_initial;
Ks = (2/3)*[cos(q) cos(q-2*pi/3) cos(q+2*pi/3);
   sin(q) sin(q-2*pi/3) sin(q+2*pi/3);
   0.5 0.5 0.5];

i2qd0 = Ks*[i_2a0_1 i_2b0_1 i_2c0_1]';
i2q_eq = i2qd0(1);
i2d_eq = i2qd0(2);
i20_eq = i2qd0(3);

i3qd0 = Ks*[i_3a0_1 i_3b0_1 i_3c0_1]';
i3q_eq = i3qd0(1);
i3d_eq = i3qd0(2);
i30_eq = i3qd0(3);

Punf = -cl*(3/2)*((i2q_eq+i3q_eq)*i2q_eq+(i2d_eq+i3d_eq)*i2d_eq);
Qunf = -cl*(3/2)*(i3d_eq*i2q_eq-i3q_eq*i2d_eq);
Vunf = (-cl/sqrt(2))*sqrt((i2q_eq+i3q_eq)^2+(i2d_eq+i3d_eq)^2);

n1 = (3/2)*cl/Tp;
n2 = (3/2)*cl/Tq;
n3 = cl/(sqrt(2)*sqrt((i2d_eq+i3d_eq)^2+(i2q_eq+i3q_eq)^2)*Tv);
```

```
%linearized matrix
M = [a11 -w a12 0 -b12*(Kp*(E1_req+mQ*Q_eq/Sbase-V_eq/Vbase)+...
z_eq)*sin(delta_eq) b12*cos(delta_eq) 0 b12*Kp*mQ*...
cos(delta_eq)/Sbase -b12*Kp*cos(delta_eq)/Vbase;
    w a11 0 a12 -b12*(Kp*(E1_req +mQ*Q_eq/Sbase-V_eq/Vbase)+...
    z_eq)*cos(delta_eq) -b12*sin(delta_eq) 0 -b12*Kp*mQ*...
    sin(delta_eq)/Sbase b12*Kp*sin(delta_eq)/Vbase;
    a21 0 a22 -w 0 0 0 0 0;
    0 a21 w a22 0 0 0 0 0;
    0 0 0 0 0 0 -Mp(m)/Sbase 0 0;
    0 0 0 0 0 0 0 Ki*mQ/Sbase -Ki/Vbase;
    -n1*(2*i2q_eq+i3q_eq) -n1*(2*i2d_eq+i3d_eq) -n1*i2q_eq...
     -n1*i2d_eq 0 0 -1/Tp 0 0;
    -n2*i3d_eq n2*i3q_eq n2*i2d_eq -n2*i2q_eq 0 0 0 -1/Tq 0;
    -n3*(i2q_eq+i3q_eq) -n3*(i2d_eq+i3d_eq) -n3*(i2q_eq+...
    i3q_eq) -n3*(i2d_eq+i3d_eq) 0 0 0 0 -1/Tv];

Eig = eig(M);
E1(n) = Eig(1);
E2(n) = Eig(2);
E3(n) = Eig(3);
E4(n) = Eig(4);
E5(n) = Eig(5);
E6(n) = Eig(6);
E7(n) = Eig(7);
E8(n) = Eig(8);
E9(n) = Eig(9);

mP = Mp(n+1);

R1_net = Rload(n+1);%#ok<NASGU>
R2_net = R_TM_high*N^2+R_TM_low;
R3_net = (Rline1+R_TG_high)*N^2+Rline2+R_TG_low;

R1a = R1_net;  R1b = R1a;      R1c = R1a;
R2a = R2_net; R2b = R2a;      R2c = R2a;
R3a = R3_net;   R3b = R3a;      R3c = R3a;

R_br = [R1a 0 0   0   0   0   0   0   0;
        0   R1b 0   0   0   0   0   0   0;
        0   0   R1c 0   0   0   0   0   0;
        0   0   0   R2a 0   0   0   0   0;
        0   0   0   0   R2b 0   0   0   0;
        0   0   0   0   0   R2c 0   0   0;
```

```
        0   0   0   0   0   0   R3a 0   0;
        0   0   0   0   0   0   0   R3b 0;
        0   0   0   0   0   0   0   0   R3c];

clear Bb_trans
[A_ss,B_ss,C_ss,D_ss] = Bb_trans(Aa,R_br,L_br);%#ok<NASGU>
a11 = A_ss(1,1);
a12 = A_ss(1,4);
a21 = A_ss(4,1);
a22 = A_ss(4,4);
b12 = B_ss(1,4);
b22 = B_ss(4,7);
cl = C_ss(10,1);

if n == Nmax || n == Nmax-2
    tstop = 1;
else
    tstop = 5/60;
end

[t1,x1,y1] = sim('basic_test_sim_111',tstop);

if n == Nmax-2
    y1_stable = y1;
    t1_stable = t1;
elseif n == Nmax
        y1_unstable = y1;
        t1_unstable = t1;
else
    y1 = y1;
end

y1_old = y1(length(y1),:);

n = n+1;
end
E6 = E6(2:length(E6));
```

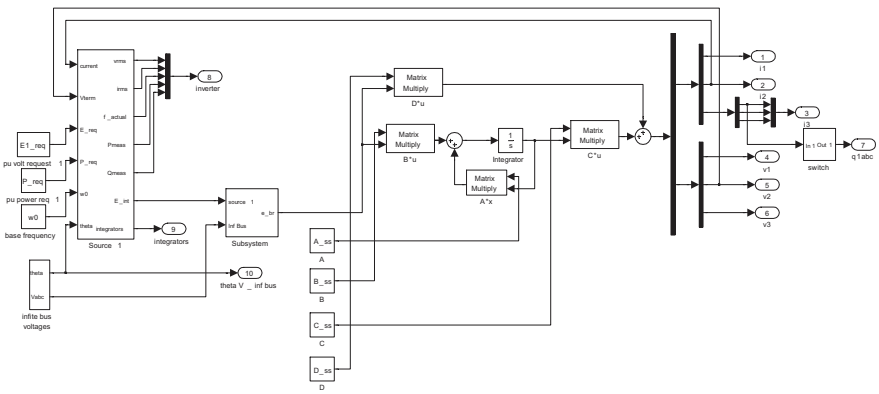

Figure C.1: Block diagram of the single-inverter microgrid used in stability analysis

REFERENCES

[1] R. Lasseter, "Microgrids," *IEEE Power Engineering Society Winter Meeting*, vol. 1, pp. 305–308, Jan. 2002.

[2] H. Nikkhajoei and R. Lasseter, "Distributed generation interface to the CERTS microgrid," *IEEE Transactions on Power Delivery*, vol. 24, pp. 305–308, July 2002.

[3] Y. Li, D. Vilathgamuwa, and P. Loh, "Design, analysis, and real-time testing of a controller for multibus microgrid system," *IEEE Transactions on Power Electronics*, vol. 19, pp. 1195–1204, Sep. 2004.

[4] N. Pogaku, M. Prodanovic, and T. Green, "Modeling, analysis, and testing of autonomous operation of an inverter-based microgrid," *IEEE Transactions on Power Electronics*, vol. 22, pp. 613–625, Mar. 2007.

[5] T. Green and M. Prodanovic, "Control of inverter-based micro-grids," *Electric Power Systems Research*, vol. 77, pp. 1204–1213, July 2007.

[6] A.Yildiz, B. Cakir, N. Inanc, and N. Abut, "A fast simulation technique for the power electronic converters," in *Applied Power Electronics Conference and Exposition*, 1999, pp. 191–196.

[7] O. Wasynczuk and S. Sudhoff, "Automated state model generation algorithm for power circuits and systems," *IEEE Transactions on Power Systems*, vol. 11, pp. 1951–1956, Nov. 1996.

[8] L. Chua and P. Lin, *Computer-Aided Analysis of Electronic Circuits: Algorithms and Computational Techniques*. Englewood Cliffs, NJ: Prentice Hall, 1975.

[9] J. Martinez and J. Martin-Arnedo, "Expanding capabilities of EMTP-like tools: From analysis to design," *IEEE Transactions on Power Delivery*, vol. 18, pp. 1569–1571, Oct. 2003.

[10] N. Soultanis, S. Papathanasiou, and N. Hatziargyriou, "A stability algorithm for the dynamic analysis of inverter dominated unbalanced LV microgrids," *IEEE Transactions on Power Systems*, vol. 22, pp. 294–304, Feb. 2007.

[11] M. Brucoli, T. Green, and J. McDonald, "Modelling and analysis of fault behaviour of inverter microgrids to aid future fault detection," in *IEEE International Conference on System of Systems Engineering*, Apr. 2007, pp. 1–6.

[12] G. Kariniotakis, N. Soultanis, A. Tsouchnikas, S. Papathanasiou, and N. Hatziargyriou, "Dynamic modeling of microgrids," in *International Conference on Future Power Systems*, Nov. 2005, pp. 1–7.

[13] D. Ariyasinghe and D. Vilathgamuwa, "Stability analysis of microgrids with constant power loads," in *IEEE International Conference on Sustainable Energy Technologies*, Nov. 2008, pp. 279–284.

[14] F. Resende and J. Lopes, "Development of dynamic equivalents for microgrids using system identification theory," *IEEE Lausanne Power Tech*, vol. 1, pp. 1033–1038, July 2007.

[15] T. Panigrahi, A. Saha, S. Chowdhury, S. P. Chowdhury, N. Chakraborty, Y. Song, and S. Byabortta, "A simulink based microgrid modelling and operational analysis using distributed generators," in *International Universities Power Engineering Conference*, Sep. 2006, pp. 222–226.

[16] L. Wang, A. Davoudi, J. Jatskevich, and P. L. Chapman, "Accelerated state-variable modeling of synchronous machine-converter systems," in *IEEE International Symposium on Circuit and Systems*, May 2008, pp. 3037–3040.

[17] J. Jatskevich, O. Wasynczuk, E. Walters, and C. Lucas, "Continuous state-space modeling of switched electric networks," in *International Conference of Control Applications*, Sep. 2000, pp. 902–907.

[18] O. Wasynczuk, E. Walters, and H. Hegner, "Simulation of a zonal electric distribution system for shipboard applications," in *Energy Conversion Engineering Conference*, July 1997, pp. 268–273.

[19] M. Barnes, J. Kondoh, H. Asano, J. Oyarzabal, G. Ventakaramanan, R. Lasseter, N. Hatziargriou, and T. Green, "Real-world microgrids - An overview," in *IEEE International Conference on System of Systems Engineering*, Apr. 2007, pp. 1–8.

[20] Y. Zhao and L. Guo, "Dynamical simulation of laboratory microgrid," in *Asia-Pacific Power and Engineering Conference*, Mar. 2009, pp. 1–5.

[21] R. Lasseter, "CERTS microgrid," in *IEEE International Conference on System of Systems Engineering*, Apr. 2007, pp. 1–5.

[22] P. Piagi and R. Lasseter, "Autonomous control of microgrids," *IEEE Power Engineering Society General Meeting*, vol. 1, pp. 1–8, June 2006.

[23] R. Tirumala, N. Mohan, and C. Henze, "Seamless transfer of grid-connected PWM inverters between utility-interactive and stand-alone modes," in *Applied Power Electronics Conference and Exposition*, vol. 2, Mar. 2002, pp. 10–14.

[24] X. Yu, Z. Jiang, and Y. Zhang, "Control of parallel inverter-interfaced distributed energy resources," in *IEEE Energy 2030 Conference*, Nov. 2008, pp. 1–8.

[25] J. Guerrero, N. Berbel, J. Matas, J. Sosa, and L. G. de Vicuna, "Droop control method with virtual output impedance for parallel operation of uninterruptible power supply systems in a microgrid," in *Applied Power Electronics Conference*, Mar. 2007, pp. 1126–1132.

[26] A. Kwasinski and P. Krein, "Multiple-input dc-dc converters to enhance local availability in grids using distributed generation resources," in *Applied Power Electronics Conference*, Mar. 2007, pp. 1657–1663.

[27] M. Pai, *Power Circuits and Electromechanics*. Champaign, IL: Stipes Publishing L.L.C., 2002.

[28] P. Schavemaker and L. van der Sluis, *Electrical Power System Essentials*. West Sussex, England: Wiley, 2008.

[29] P. Krause, O. Wasynczuk, and S. Sudoff, *Analysis of Electric Machinery and Drive Systems*. Piscataway, NJ: IEEE Press, 2002.

[30] R. Lasseter and P. Piagi, "Control and design of microgrid components," Power Systems Engineering Research Center, Madison, WI, Tech. Rep. Publication 06-036, Jan. 2006.